arXiv:1401.1194v2 [astro-ph.SR] 9 Feb 2014

WISE Y Dwarfs As Probes of the Brown Dwarf-Exoplanet Connection

C. Beichman[1,2,3], Christopher R. Gelino[1,3], J. Davy Kirkpatrick[1], Michael C. Cushing[4], Sally Dodson-Robinson[5], Mark S. Marley[6], Caroline V. Morley[7], and E.L. Wright[8]

1) Infrared Processing and Analysis Center, California Institute of Technology, Pasadena CA 91125

2) Jet Propulsion Laboratory, California Institute of Technology, 4800 Oak Grove Dr., Pasadena CA 91107

3) NASA Exoplanet Science Institute, California Institute of Technology,770 S. Wilson Ave., Pasadena, CA 91125

4) Department of Physics and Astronomy, The University of Toledo, 2801 West Bancroft Street, Toledo, OH 43606

5) Department of Astronomy, University of Delaware, Newark, DE 19716

6) NASA Ames Research Center, Mountain View, CA 94035

7) Department of Astronomy, University of California at Santa Cruz, Santa Cruz, CA 95064

8) Department of Astronomy, University of California Los Angeles, PO Box 951547, Los Angeles CA 90095

chas *at* ipac.caltech.edu

ABSTRACT

We have determined astrometric positions for 15 WISE-discovered late-type brown dwarfs (6 T8-9 and 9 Y dwarfs) using the Keck II telescope, the *Spitzer Space Telescope*, and the *Hubble Space Telescope*. Combining data from 8 to 20 epochs we derive parallactic and proper motions for these objects which put the majority within 15 parsecs. For ages greater than a few Gyr, as suggested from kinematic considerations, we find masses of 10-30 M_{Jup} based on standard models for the evolution of low mass objects with a range of mass estimates for individual objects depending on the model in question. Three of the coolest objects have effective temperatures $\sim$ 350 K and inferred masses of 10-15 M_{Jup}. Our parallactic distances confirm earlier photometric estimates (Kirkpatrick et al. 2012) and direct measurements (Marsh et al. 2013; Beichman et al. 2013; Dupuy & Kraus 2013) and suggest that the number of objects with masses below about15 M_{Jup} must be flat or declining relative to higher mass objects. The masses of the coldest Y dwarfs may be similar to those inferred for recently imaged planet-mass companions to nearby young stars. Objects in this mass range, which appear to be

rare in both the interstellar and proto-planetary environments, may both have formed via gravitational fragmentation: the brown dwarfs in interstellar clouds and companion objects in a protoplanetary disk. In both cases, however, the fact that objects in this mass range are relatively infrequent, suggests that this mechanism must be inefficient in both environments.

Subject headings: brown dwarfs Astrometry - Parallaxes - proper motions - solar neighborhood

1. Introduction

Our understanding of the gravitational collapse of interstellar gas clouds to form stars is one of the great success stories of modern astrophysics. The discovery of "protostars" in molecular clouds via infrared and millimeter observations started with high luminosity stars in giant molecular clouds, e.g. the Becklin-Neugebauer (Becklin & Neugebauer 1967) and Kleinmann-Low (Kleinmann & Low 1967) objects in the Orion Molecular Cloud (Wilson et al. 1970) and progressed steadily through to the discovery of young stars of solar mass in clouds like Taurus (Beichman et al. 1986) and to objects of still lower masses with Spitzer (Dunham et al. 2013). The theory of star formation progressed hand in hand with observations, from initial discussions of the cloud collapse (Larson 1985) to detailed models incorporating disks and outflows (Shu et al. 1987). Long standing questions in star formation theory concern the distribution of stellar masses (the Initial Mass Function, IMF) produced by this process and the end-points of the process, i.e. the largest and smallest self-gravitating objects that can be formed via gravitational collapse. The discovery of substellar objects, "brown dwarfs," orbiting nearby stars (Nakajima et al. 1995) and in early sky surveys, e.g. The Two Micron All sky survey (2MASS; Skrutskie et al. 2006), DEep Near Infrared Southern Sky Survey (DENIS; Epchtein et al. 1997) and Sloan Digital Sky Survey (SDSS; York et al. 2000) pushed the low mass limit of the IMF well below the 0.07 $M_{\odot}$ stellar limit (Kirkpatrick et al. 1999; Kirkpatrick 2005). Data from the UKIRT Infrared Deep Sky Survey (UKIDSS) added many new L and T dwarfs and improved our knowledge of their space densities (Burningham et al. 2013). Most recently, the launch of the Wide-field Infrared Survey Explorer (WISE; Wright et al. 2010) has led to the identification of over 250 brown dwarfs with extremely low effective temperatures, T_{eff}, including the first Y dwarfs with $T_{eff} \sim$ 250-500 K (Kirkpatrick et al. 2011, 2012; Cushing et al. 2011).

In the early 1980's, before the advent of theories of non-baryonic dark matter, it was thought that sharply increasing low mass stellar and brown dwarf mass functions could account for the local missing mass inferred from galaxy rotation curves (Bahcall & Casertano 1985). This conjecture was ultimately ruled out as the shape of the low mass IMF was determined with results from the Hubble Space Telescope (HST) (Flynn et al. 1996), SDSS and 2MASS, as well as by the incidence of microlensing events determined by the MACHO project (Alcock et al. 1996). Thus, while the low

mass shape of the IMF is no longer of cosmological importance, it remains an important question for star formation theory and role of gravitational instability in the origin of the IMF. A related question about gravitational instability arises due to the existence of planetary mass companions on extremely wide orbits, e.g. HR 8799 and Fomalhaut (Marois et al. 2008; Kalas et al. 2004) which is difficult to reconcile with models of planet formation via core accretion (Dodson-Robinson et al. 2009). The formation of low mass objects via gravitational instability appears to be important in the proto-planetary environment as well.

Thus, we investigate Y dwarfs found with WISE as probes of the low mass IMF and as analogs to the massive planets orbiting nearby stars. Our long term goals are to understand better the physical properties of these objects and to assess how they might form, in either the interstellar or proto-planetary environments. A key step toward this goal is to determine the distances to the closest, lowest mass objects found by WISE. The first paper in this program reported a parallax for one of the coldest WISE Y dwarfs, WISE1828+2650, classified as a $\geq$Y2 object with a temperature of $\sim$300-500 K and a mass of $\sim$ 5 M_{Jup} for an assumed age of $\sim$5 Gyr (Beichman et al. 2013). We report here on parallax determinations of 15 WISE objects with spectral types of T8 or later made using imaging with the Hubble Space Telescope (*HST*), the *Spitzer Space Telescope*, and the Keck-II telescope. In what follows, we define the sample (§2), describe the observations (§3) and derive the kinematic parameters (§4). In §5 we use the spectral energy distribution and absolute magnitudes to estimate the masses of the Y dwarfs, address the possible ages of the sample objects on the basis of their kinematic properties, and discuss the apparent cutoffs in the distributions of brown dwarf and planetary companions in the range of $<$15 M_{Jup}.

2. The Sample

One of the key goals of the WISE mission was the detection of ultra-cool T and Y brown dwarfs with the properties of the instrument tailored such that the W2 filter at 4.6 μm was positioned to sit at the peak of the cool brown dwarf spectral energy distribution while the shorter wavelength W1 filter at 3.5 μm sits in a region of methane absorption (Burrows et al. 1997). Thus, the prominent red W1-W2 color of brown dwarfs makes them relatively easy to identify among the millions of WISE sources so that the objects studied in this paper (Table 1) are selected primarily for their extreme color, W1-W2$>$ 2.5 mag (Kirkpatrick et al. 2011, 2012; Cushing et al. 2011; Mace et al. 2013; Cushing et al. 2013). Approximately 17 Y dwarfs are presently known, including field objects from WISE, a T dwarf companion (Liu et al. 2012), and a white dwarf companion[1] (Luhman et al. 2011). In this paper we study nine WISE field Y dwarfs as well as six slightly warmer, late T dwarfs.

[1]The Spitzer colors and absolute magnitude suggest a Y dwarf classification, but no confirming spectrum has yet been obtained.

As discussed in Kirkpatrick et al. (2012) we suggest that the Y dwarf sample discussed here is relatively complete at the WISE W2 magnitude limits appropriate to low ecliptic latitudes. While the V/V_{max} value of 0.3 indicates that the late T and Y dwarf sample out to 10 pc are modestly incomplete (Kirkpatrick et al. 2012; Schmidt 1968), a number of investigations are underway to identify additional Y dwarfs with WISE, including improved processing and more follow-up observations. The sample studied here of 9 Y dwarfs limited only by a declination limit of $\delta > -36^o$, represents a large fraction of the available Y dwarfs from WISE. An additional 6 objects, late T dwarfs, were included in the sample to help to elucidate the transition between these two spectral types.

3. Observations

As described in Beichman et al. (2013) we piece together positional information with a variety of telescopes in the 1-5 μm range. In the near-infrared where the Y dwarfs are intrinsically faint, we have used the Keck-II telescope with laser guide star adaptive optics and, for nine objects, the Hubble Space Telescope (HST). In the 3-5 μm range where the sources are much brighter, we have the original WISE measurements which are of low positional accuracy as well as Spitzer observations which offer higher resolution and higher signal to noise ratio (SNR). Individual positional uncertainties with the various telescopes range between 5-10 mas (Keck and HST), 60 mas (Spitzer) and 250-500 mas (WISE). We then have to tie together multiple astrometric reference frames which adds an additional layer of positional uncertainty. While this multiplicity of telescopes presents the challenge of matching astrometric reference frames, we gain the advantage of a long temporal baseline and denser sampling of the Y dwarf motions that would be difficult to achieve with a single facility. Table 1 lists the WISE sources, their spectral types, and the number of observations with a particular facility. Table 2 gives the observing log for each facility as well the astrometric data at each epoch (§4).

3.1. WISE Observations

The WISE mission had three distinct phases: the 4-band cryogenic period, the 3-band cryogenic period, and 2-band warm mission. Depending on position on the sky, especially ecliptic longitude, sources were observed in one or more of these phases. We determined positions and magnitudes for each period separately with a median date of observation spanning 1-2 days. Positions and associated uncertainties were obtained by averaging the source positions in the multi-band extractions from each individual orbit. The uncertainty in the WISE astrometric frame is approximately 80 mas based on the input 2MASS catalog used for WISE position reconstruction (Cutri et al. 2011). Typically, however, the positional uncertainties in the WISE detections are much larger than this, $\sim$250-500 mas, due to its large beamsize and detection at only one or at most two wavelengths, or to the effects of confusion with other nearby objects.

In Table 3 we report averages of the 4.5 μm magnitudes (W2) for the various epochs and include 3.5 μm (W1) when available. Upper limits in the two longer wavelength bands, 12 (W3) and 22 μm (W4) are high and do not significantly constrain the spectral energy distributions. We have converted the magnitudes to flux densities using the zero points from Wright et al. (2010), but because of the unknown and extremely non-blackbody-like nature of brown dwarf spectral energy distributions (SED), we have not color-corrected these flux densities. Table 4 indicates that there is no evidence for variability in the [4.6] magnitudes at the 2-3 % level for any of these objects. While not varying in the Spitzer bands, WISE2220-3628 shows evidence for variability in the comparison of the ground-based J and HST/F125W photometry, with a nearly 1 mag difference between the two bands. Further monitoring of this object may be warranted.

3.2. HST Observations

Nine objects were imaged with HST's WFC3/IR in the F105W, F125W or F140W filters as precursor observations in support of subsequent grism measurements. The final images are quite heterogeneous, consisting of from one to four dithered exposures with exposure times ranging from 312 to 2412 seconds. In some cases multiple exposures were taken with small offsets to reduce the effects of cosmic rays and the undersampling of the individual frames. The Space Telescope Science Institute's (STScI) "AstroDrizzle" mosaic pipeline was used to process these data to produce final mosaicked images. The pipeline corrects for the geometric distortion of the WFC3-IR camera to a level estimated to be ~ 5 mas (Kozhurina-Platais et al. 2009) which is of the same order or less than the extraction uncertainties of the faint target. Sources were extracted using the Gaussian-fitting IDL FIND routine to determine centroid positions and the APER routine[2] with a 3 pixel radius for photometric measurements. The Full Width at Half Maximum (FWHM) for these undersampled data is ~ 2 pixels or $0.26''$ consistent with STScI analyses (Kozhurina-Platais et al. 2009). Analysis of fields with multiple HST observations, e.g. WISE1541-2250, shows that after registration onto a common reference frame, the repeatability of individual source positions is ~ 5 mas for bright objects located within $90''$ of the brown dwarf. The photometry was calibrated using the appropriate zero-points for Vega magnitudes[3] from the WFC3 Handbook (Rajan 2010).

3.3. Spitzer Observations

Observations with the *Spitzer Space Telescope* were made using a variety of General Observer (GO) programs (PI D. Kirkpatrick) and some Director's Discretionary Time (A. Mainzer and T.

[2]All the photometric measurements reported herein were made using this routine from the IDL ASTRO library, http://idlastro.gsfc.nasa.gov/contents.html. A number of other IDL routines are taken from this library as well.

[3]http://www.stsci.edu/hst/wfc3/phot_zp_lbn

Dupuy). In all cases the observations were obtained during the Warm Mission phase using the IRAC camera (Fazio et al. 2004) in its full array mode to make observations at 3.6 (Channel-1) and/or 4.5 μm (Channel-2). We analyzed post-BCD mosaics from the Spitzer Science Center (SSC) to make photometric and astrometric measurements, extracting sources using a 4 pixel radius aperture, a 4-12 pixel annulus for sky subtraction, and normalizing the resultant counts using SSC-recommended aperture corrections[4].

For each target we put all epochs of Channels-1 and -2 onto a common reference frame by averaging the positions of all bright sources within ∼60-90″ of the target, typically 25-50 objects per frame, and calculating small offsets from one epoch to the next to register all frames to the average value. The largest offsets were of order 200 mas and typically much smaller, around 50 mas. We kept the size of the overlap region smaller than the overall size of the IRAC field of view to minimize the effects of optical distortion. The dispersion around the average bright source position is typically 60 mas in both right ascension and declination, or $1/20^{th}$ of the native 1.2″ pixel (Figure 1). These values are less than 100 mas distortions quoted by the SSC[5] in part because we have confined our observations to the small regions at the center of the IRAC arrays. Figure 1 shows the positional uncertainty in multiple observations (N_{obs}=2 to 13) for 800 reference sources from all of our target fields as a function of IRAC [4.6] magnitude. These single axis uncertainties have been normalized to a single epoch according to $N_{obs}^{1/2}$ and are thus representative of the uncertainties for our single epoch brown dwarf measurements. The final positions for reference sources are improved relative to these values by $N_{obs}^{1/2}$. The solid line shows a simple model to the positional uncertainty with a constant value of 58±8 mas for sources brighter [4.6]=17.6±0.2 mag and a value which increases monotonically as SNR^{-1} to fainter levels (Monet et al. 2010). Our bright brown dwarf targets are always in the flat part of the uncertainty distribution.

3.4. Keck NIRC2 Observations

Targets were observed in the H-band using using NIRC2 on the Keck-2 telescope with the laser guide star Adaptive Optics (AO) system (Wizinowich et al. 2006; van Dam et al. 2006) and tip-tilt stars located 10-50″ away. The wide-field camera (40 mas/pixel scale; 40″ field of view) was used to maximize the number of reference stars for astrometry. At each epoch, dithered sequences of images with offsets of 1.5″–3″ in right ascension or declination and total integration times of 1080 sec were obtained at airmass of 1.0-2.0. The majority of sources were observed at airmasses < 1.5. The individual images were sky-subtracted with a sky frame created by the median of the science frames and flat-fielded with a dome flat using standard and custom IDL routines. Individual images were "de-warped" to account for optical distortion in the NIRC2 camera

[4]The post-BCD images have 0.6″ pixels derived from the 1.22″ native pixel data. The aperture correction is described in http://irsa.ipac.caltech.edu/data/SPITZER/docs/irac

[5]http://irsa.ipac.caltech.edu/data/SPITZER/docs/irac/iracinstrumenthandbook/26/

(Beichman et al. 2013). The reduced images were shifted to align stars onto a common, larger grid and the median average of overlapping pixels was computed to make the final mosaic. The source positions obtained from the Keck images were corrected for the effects of differential refraction relative to the center of the field using meteorological conditions available at the CFHT telescope weather archive[6] to determine the index of refraction corrected for wavelength, local temperature, atmospheric pressure and relative humidity (Lang 1983) and standard formulae (Stone 1996). As discussed in Beichman et al. (2013), for the small field of view of the NIRC2 images and the relatively low airmasses under consideration here, the first order differential corrections are small, <10 mas across the $\pm 20''$ field and proportionately less at smaller separations.

The effects of optical distortion in the wide-field NIRC2 camera were corrected using a distortion map derived by comparing Keck data of the globular cluster M15 (Alibert et al. 2005). Details of this distortion mapping are described in (Beichman et al. 2013) but the correction amounts to < 1 pixel (40 mas) across most of the array and up to 2 pixels at the edges of the array. After our correction procedure the residual distortion errors are less than 10 mas over the entire field.

4. Astrometric Data Reduction

The first step in determining the position of a target is to put all the available datasets onto a common reference frame. When HST observations were available, sources seen in common between HST and Spitzer were used to register the two fields onto a common frame with a typical accuracy of < 20 mas, considerably less than the uncertainty in Spitzer positions themselves (50-60 mas). We used HST and Keck images to reject obviously extended objects from consideration as obtaining a good centroid position for these objects can be difficult, particularly in Keck images. However, whenever possible, objects with only slight extent ($<0.2''$) were included since these extragalactic sources help to anchor the positions to an absolute reference frame.

The Keck fields were referenced to the HST or HST/Spitzer reference frame using from 3 to 10 objects seen in common in the $40''$ field of view of NIRC2. The accuracy of this registration varied from 3-30 mas (Table 5) with the number of reference objects and the quality of the night. Images showing HST, Spitzer and Keck fields are shown in Figures 2-Figurew2220image with the positions of some of the reference stars indicated in green. While the rotational orientation of the Spitzer and HST frames are well determined in their respective pipelines ($<0.001^o$) and thus has little effect on derived positions, the same cannot be said for the Keck images. We determined the rotation using the HST and/or Spitzer reference stars with an accuracy that varies between 0.005^o up to 0.05^o, depending on the number of stars and the quality of the night. The effect of this rotational uncertainty is included in the assignment of the uncertainty in the position of the brown dwarf.

[6] http://mkwc.ifa.hawaii.edu/archive/wx/cfht/

Finally, although the absolute coordinate system is not directly relevant to the determination of parallax and proper motions, we note that we have adopted the Spitzer frame in our quoted positions. The Spitzer positions are based on the 2MASS catalog as is the WISE coordinate system (Cutri et al. 2011). The estimated global accuracy of the 2MASS frame is estimated to be approximately 80 mas (Skrutskie et al. 2006).

4.1. Determination of Parallax and Proper Motion

Table 2 lists the positions for the WISE targets for each available epoch. The right ascension and declination data were fitted to a model incorporating proper motion and parallax (Smart 1977; Green 1985):

$$\begin{aligned} \alpha' &\equiv \alpha_0 + \mu_\alpha(t - T_0)/cos(\delta') \\ \delta' &\equiv \delta_0 + \mu_\delta(t - T_0) \end{aligned} \quad (1)$$

$$\begin{aligned} \alpha(t) &= \alpha' + \pi\Big(X(t)sin\,\alpha' - Y(t)cos\,\alpha'\Big)/cos\,\delta' \\ \delta(t) &= \delta' + \pi\Big(X(t)cos\,\alpha' sin\,\delta' + Y(t)sin\,\alpha' sin\,\delta' - Z(t)cos\,\delta'\Big) \end{aligned} \quad (2)$$

where (α_0, δ_0) are the source position for equinox and epoch T_0 =J2000.0, $\mu_{\alpha,\delta}$ are proper motion in the two coordinates in $''$/yr, and π is the annual parallax in arcsec. The coefficients $X(t)$, $Y(t)$, and $Z(t)$ are the rectangular coordinates of the observatory as seen from the Sun in AU. Values of X, Y, Z for the terrestrial or Earth-orbiting observatories are taken from the IDL ASTRO routine XYZ while X, Y, Z values for the earth-trailing *Spitzer* observatory are obtained from the image headers provided by the SSC. Equations (1) and (2) are solved simultaneously using the *Mathematica* routine *NonLinearModelFit*[7] incorporating appropriate uncertainties for each data-point.

The solutions are given in Table 6 with precisions for the derived parallax values ranging from 5% (WISE1541-2250) up to indeterminate values with uncertainties of 50% (WISE 0836-1859). Figures 17 to 24 show the fit to the total motion of the sources (proper motion plus parallax) as well as the fit to the motion with both proper motion and the effect of observatory location (terrestrial or Earth-trailing) removed. Our determinations are robust for 12 objects (uncertainties $< 15\%$) with an average distance of 8.7 pc and a maximum distance for a well determined distance of 15 pc. Three objects (WISE0836-1859, WISE1542+2230, WISE2220-3628) have low precision parallaxes due to either a small number of measurements, in particular with Keck or HST and/or a sparse set of reference stars. For the first two objects it is likely that the true distance for these

[7]http://reference.wolfram.com/mathematica/ref/NonlinearModelFit.html

T dwarfs is greater than 15 pc and thus more challenging to determine. For the 13 objects showing uncertainties less than 20% (and 12 objects with uncertainties <15%) we are relatively immune to the Lutz-Kelker bias in our determination of absolute magnitudes or other derived quantities. The bias occurs when more objects at larger distances are scattered into a sample than when objects of smaller distances are scattered out of the sample (Lutz & Kelker 1973).

These parallaxes are determined relative to small groups of objects (typically stars) and not tied directly to an absolute reference frame. Thus our parallaxes are relative measurements and may have biases at the < 5 mas level (Dupuy & Liu 2012) which represents a limiting floor to the accuracy of our quoted distances. Mitigating against this problem are the large parallactic values ($\sim$100 mas) for sources located within 10-15 pc as well as the fact that each field typically contains one or more extragalactic sources which help to anchor the coordinate system in an absolute sense (Mahmud & Anderson 2008).

The distance estimates determined herein are, on average, close to those presented in Kirkpatrick et al. (2012). A source-by-source comparison (Table 7) gives the ratio of the Kirkpatrick (2012) values to the ones determined here. For the late T and Y dwarfs, Kirkpatrick et al. (2012) list only a few trig parallaxes (Marsh et al. 2013) with the majority coming from photometric distances determined by comparing source brightness in the H and WISE W2 bands with color-magnitude diagrams for those few T and Y dwarf objects with measured parallaxes. For the 12 sources with Keck distance errors <20%, the Kirkpatrick/Keck distance ratio is 0.9 with a dispersion 0.2 and mean uncertainty of 0.06. This close agreement indicates that the photometric parallaxes are, in general, adequate to predict a distance within 25%. More importantly, the agreement in the average distances implies that the conclusions about the luminosity and mass functions for these ultra-low mass late T and Y dwarfs presented in Kirkpatrick et al. (2012) remain valid and now rest on more solid footing with these more precise distances.

Finally, we note that Dupuy & Kraus (2013) have recently published parallaxes for 6 objects in common with our sample. Table 8 demonstrates good agreement (1-2 σ) between their parallax and proper motions in all but one case, WISE 1541-2250, which differs by 3 σ. Examination of the Spitzer data for this object shows significant contamination with a nearby star as the WISE object approaches the star. We simultaneously fitted Gaussian profiles of the same width to the two sources for sightings when the sources were far enough apart to distinguish cleanly. For observations after MJD=56066, we were unable to make an accurate determination and did not use Spitzer data in our fitting. However, the WISE object and the star are cleanly delineated in the early Spitzer observations and most importantly in our high resolution Keck and HST data, leading us to trust our solution which puts the object at 5.7$\pm$0.3 pc instead of Dupuy & Kraus's more distant 13.5$\pm$5.6 pc. A few more observations, especially after the object clears the offending star, will put the distance to this object on a firm footing.

5. Discussion

5.1. Spectral Energy Distributions

We have used published models which predict the spectral energy distributions (SED) of our sources to investigate their physical properties. We acknowledge at the outset that this discussion is fraught with danger given the known difficulties with modeling brown dwarfs with effective temperatures T_{eff} << 1000K and sometimes <400 K. Developing models at these low temperatures is very much an on-going task requiring new gas and dust opacities as well as incorporating clouds of water and metallic precipitates, and possibly non-equilibrium chemistry (Baraffe et al. 2003; Morley et al. 2012; Marley et al. 2007). In addition to the intrinsic model uncertainties, the models are degenerate between mass and age since the temperature and luminosity of a brown dwarf decrease slowly with time. Thus a source with a particular SED, i.e. with some T_{eff}, could be either a young, low mass object or an older, more massive one. With these caveats in mind we examined two different sets of models, the dust-free BT-Settl models (Allard et al. 2003, 2010) with opacities updated relative to the older COND models (Baraffe et al. 2003) and a series of models (hereafter denoted "Morley" models) incorporating sulfide and chloride clouds as well as a cloud-free case (Morley et al. 2012; Leggett et al. 2012; Saumon & Marley 2008). The Morley models are characterized by the amount of sedimentation of the precipitated material, according to a parameter f_{sed}, ranging from $2 < f_{sed} < 5$ and as well as a cloud-free case. A higher value of f_{sed} corresponds to optically thinner clouds while a lower f_{sed} corresponds to optically thicker clouds. Neither of these models include non-equilibrium chemistry or the influence of water clouds, although the effects of water condensation are included in the model.

The models tabulate absolute magnitudes for a variety of filters, including ground-based (MKO) J and H, HST F125W and F140W, as well as Spitzer Channels 1 and 2 ([3.6] and [4.5] μm). We calculated a χ^2 value based on absolute [4.5] μm flux density using the Spitzer Ch2 photometry and our distance estimate as well as up to 5 photometric colors: J-[4.5], H-[4.5], [F125W]-[4.5],[F140W]-[4.5] and [3.6]-[4.5].

$$\chi^2 = \frac{(Abs[4.5]_{obs} - Abs[4.5]_{model})^2}{(5/ln(10)\sigma_D/D)^2 + \sigma([4.5])_{obs})^2} + \sum_i \frac{((mag_i - [4.5])_{obs} - (mag_i - [4.5])_{model})^2}{\sigma(mag_i)^2 + \sigma([4.5])^2_{obs}}) \quad (3)$$

where D is the distance to the source, $Abs[4.5] = [4.5] - 5 \times \log(D/10pc)$ is the absolute 4.5 μm magnitude, and mag_i is the magnitude in the relevant band. The minimum χ^2 values for each source were determined through the interpolated (mass, age) grid with (0.1 Gyr < Age < 10 Gyr, 5 <Mass< 80 M_{Jup}) for the BT-Settl models, yielding the model parameters in Table 9. For the

coldest Y dwarfs, the data suggest $T_{eff} < 400$K and in these cases we used a coarser grid of BT-Settl models, sampling ($300K < T_{eff} < 400K$ and $3.0 < log\,g < 5.5$) for an assumed radius of 1 R_{Jup} and where $log\,g$ is the log of the surface gravity. For the Morley models, we interpolated in a (T_{eff},$log\,g$) grid for discrete values of f_{sed}. The solution spaces for each source, Log(χ^2) as a function of model parameters, are shown in Figure 25 and Figure 26. Tables 9 and 10 give the fitted values for each source with their associated uncertainties derived from a Monte Carlo analysis in which the distances and photometric values were varied according to their nominal uncertainties. For the cold BT-Settl cases, the uncertainties reflect the coarseness of the grid, not the observational uncertainties. The tables include values of radius and *log g* from the appropriate evolutionary tracks as well as the χ^2 of the fits. Table 10 also includes the differences in the derived values of T_{eff}, mass, and age between the Morley and BTSettl models.

The BT-Settl models (Figure 25) show a valley of preferred values in the (mass,age) plane with quite good fits ($\chi^2 < 10$ with 2-3 degrees of freedom) for some of the sources with a median value of χ^2 =22 for 2-3 degrees of freedom. For the coolest sources, i.e. WISE 1828+2650 (≥Y2), WISE1541-2250 (Y0.5) and WISE 2209+2711 (Y0:), the fits converge on T_{eff}= 350K and $log\,g$=4.5 with $\chi^2 > 400$. Figure 27a-o show the best fitting BT-Settl models. Generally, the BT-Settl solutions have a broad range of masses from 12-28 M_{Jup} with an average of 20 ± 6 M_{Jup} and ages from 3.4-8.8 Gyr with an average of 7 ± 2 Gyr. The Y dwarfs have lower masses and temperatures than the T dwarfs, 15 vs 25 M_{Jup}, and 390 K vs. 580 K. Figure 28 shows the range in temperature for the late T and Y dwarfs derived from the two sets of models.

Overall, the Morley models fit the data less well with a median value of χ^2 (with 2 or 3 degrees of freedom) of 47 compared with 22 for the BT-Settl models. These models have uniformly high surface gravities, *log g*∼ 5, at the high end of the input grid and thus yield higher masses than BT-Settl cases, ∼30 M_{Jup} in many cases. In fact, if the model grid is allowed to extend to *log g*=5.5, then the masses approach 60 M_{Jup} with ages of 15 Gyr which do not seem reasonable. The difficult sources to fit with the BT-Settl models, e.g. WISE1828+2650 and WISE1541-2250, have high χ^2values with the Morley models as well. The derived effective temperatures in the two sets of models (Morley vs. BT-Settl) are similar with the Morley models being 80 K warmer (Figure 28).

As noted in Beichman et al. (2013), WISE1828+2650 resists simple modeling due to the large disparity between the short and long wavelength magnitudes with H-[4.5]=8.1 mag. While the 3-5 μm data alone yield a good fit to a BTSettl model ($Teff$=440 K, $log\,g$ =4.5), such a model fails by ∼3 magnitudes to fit the shorter wavelength data. Similarly, fitting only the short wavelength data yields a BT-Settl model ($Teff$=300, $log\,g$ =4.5) which fails to reproduce the longer wavelength observations by comparable amounts. Adding extinction due to a very thick cloud layer with the absorption properties of "interstellar grains" suppresses the near-IR bands relative to the longer wavelengths and results a model ($Teff$=474 K, $log\,g$ = 4.6, A_V = 19 mag) with a significantly better χ^2=202 (3 d.o.f.) than the model without extinction, χ^2 = 3700 (4 d.o.f.). Adding a cloud layer also improved the BT-Settl fit for WISE 2209+2711 ($Teff$=420 K, $log\,g$ = 4.8, A_V = 15 mag) with a χ^2=123 (2 d.o.f.). Figure 27 shows these extincted models as dotted lines for these

two objects. Some previously unmodeled aspect of atmospheric physics or evolutionary status that results in a strongly absorbing cloud layer may prove necessary to understanding these objects.

It is worth noting that the poor model fits for the coldest sources are not improved by invoking a binary brown dwarf system. Fits to objects of common age but disparate masses did not show any improvement relative to the single object solutions. Nor is the juxtaposition of two unrelated sources a palatable solution since there is no evidence for one stationary and one moving object in the imaging data. similar to the putative Y dwarf companion to WD 0806-661 (Luhman et al. 2012), objects like WISE 1828+2650 and WISE1541-2250 must be underluminous at short wavelengths (or over-luminous in the long-wavelength bands) due to some as yet poorly understood aspect of these very cold atmospheres.

Figure 29 compares the data with a number of models in two color-magnitude diagrams, J vs. J-H and [4.5] vs. [3.6]-[4.5]. Deviations in both color spaces are apparent with the BT-Settl models (orange, dot-dashed) and the Morley models bracketing most of the objects in Spitzer/WISE bands. The BT-Settl models tend to be ∼1 mag bluer at a given absolute magnitude than is observed, or 1-2 mag underluminous than observed at a given [3.6]-[4.5] color. Three varieties of Morley models are shown, one cloud-free, one with sulfide clouds (f_{sed}=5, Table 10) and one incorporating water clouds (Morley et al., in preparation). The Morley models tend to be 1 mag redder than the observations at a given absolute magnitude, or 1 mag overluminous at a given color. Taken as a group, the Morley and BT-Settl models straddle the observations, but few of the models can be taken as providing a good fit, particularly for the less luminous, colder cases. There is a much wider divergence between the models and the observations in the JH color-magnitude diagram. These figures also include models incorporating water vapor clouds (Morley et al., in prep). The BT-Settl models provide a good fit to the J-H colors and absolute magnitudes for the warmer objects, while the Morley objects do a better job on the colder objects at these wavelengths. WISE 1828+2650 stands out as extremely red in J-H and is poorly fitted in any of the models.

Finally, there are a number of conclusions to be drawn from this discussion. The BT and Morley models provide reasonable fits to the properties of the warmer T dwarfs, with the cloud-free BT-Settl models providing the best representation of the absolute magnitudes and colors. But the coldest objects are difficult to fit and thus properties such as mass and age are quite uncertain. In some cases masses ∼ 10-15 M_{Jup} are close to the range inferred for the objects ("planets") found to be orbiting nearby stars, but precise determinations of masses and other properties may simply be impossible using broad photometric bands. Even determining an effective temperature using a bolometric luminosity (Dupuy & Kraus 2013) requires a bolometric correction that is model dependent and, as we have seen, quite uncertain. High resolution spectroscopy with JWST across the 1-10 μm band would yield unambiguous information on surface gravity and composition and would greatly improve our understanding of these objects. In addition, anchoring these models with a few sources with known ages and masses is absolutely critical. This can be accomplished by studying brown dwarfs in binary systems or investigating objects with higher mass companions of known ages, e.g. the potential Y dwarf companion to the white dwarf WD 0806-661 (Luhman et al.

2012).

5.2. Age of Sample

We have no direct indication of the ages of our sample. The BT-Settl and Morley models are consistent with higher surface gravity, higher mass and thus older ages of a few Gyr or more. Because independent age estimates are important because of the Mass-Age degeneracy, we use the kinematic information to make a crude estimate of the ages of these stars. The tangential velocity of each object comes from its proper motion and distance: $v_{tan} = 4.74\mu/\Pi$ km s^{-1} where μ is the total proper motion and Π the parallax (Smart 1977). For 12 objects with distance uncertainty less than 15%, the average value of v_{tan} is 34 km s^{-1} with a dispersion of 24 km s^{-1}, which falls within the distribution of tangential velocities measured for nearby (< 20 pc) L and T brown dwarfs (Faherty et al. 2009). There are, however, significant outliers in this distribution. WISE 0313+7807 has a remarkably small proper motion, 110 mas yr^{-1}, and thus a very small $v_{tan} = 3 \pm 1$ km s^{-1}. At the other extreme, WISE 0410+1502 and WISE 2209+2711 have $v_{tan} = 72 \pm 4$ km s^{-1} and 59±4 km s^{-1}, respectively. WISE0335+4310 has the most extreme proper motion, $v_{tan} = 78 \pm 10$ km s^{-1}.

These tangential velocities are consistent with M7-T9 objects studied by Faherty et al. (2009) suggesting that the extreme T and Y dwarfs studied here are drawn from the same kinematic population. For their 20 pc sample, Faherty et al. (2009) suggested ages of 2-4 Gyr for the objects with $v_{tan} < 100$ km s^{-1}. An object with a high v_{tan} like WISE 0335+4310 might be somewhat older, up to 8 Gyr. Faherty et al. (2009) suggested that a subset of their sample with low proper motions were younger than the average, perhaps <1 Gyr. Thus, the object with the lowest v_{tan}, WISE 0313+7807, might be younger than the other sources. Yet its BT-Settl model age is 9 Gyr and a low SNR spectrum of WISE 0313+7807 (Kirkpatrick et al. 2011) does not reveal any obvious peculiarities. The BT-Settl ages are all around 4-9 Gyr and thus consistent with the ages suggested by the kinematics.

Without radial velocity (RV) information it is impossible to rule definitively on the association of any of these objects with nearby clusters. Beichman et al. (2013) described a search in RV space for $V_z = \pm 100$ km s^{-1} to look for potential associations with nearby, young clusters[8] (Zuckerman & Song 2004). With one exception, none of the sample show a plausible kinematic membership with nearby clusters. If WISE 1804+3117 were to have $V_z \sim -20$ km s^{-1}, an association with Tucanae/Horologium would be possible, but since the age of this object from model fitting is ∼5 Gyr, an association with this 30 Myr old cluster would be problematical.

[8]Argus/IC2391, TW Hydrae, Tucana/Horologium, β Pictoris, AB Doradus, hCha, Cha-near, Columba and the Hyades. See Beichman et al. (2013)

5.3. Brown Dwarfs or Free Floating Planets?

The incidence of planetary-mass, field brown dwarfs is small. Within 10 pc the RECONS database (Henry et al. 2006) shows 376 objects in 259 systems as of 2012. Of these objects, 248 are M stars, 16 are T8-T9.5 objects (Kirkpatrick et al. 2012) and 11 are Y dwarfs. Thus extremely low mass objects represent just 7% of the local population of objects. For the best-fitting BT-Settl models (Table 9) there are only 5 Y dwarfs with masses < 15 M_{Jup}. While these mass estimates are obviously speculative and model dependent, it is clear that objects with masses less than $\sim$ 15 M_{Jup} form only a small percentage of the local population. The ratio of local (<10 pc) M dwarfs ($75 < M < 600$) M_{Jup} to low mass brown dwarfs ($5 < M < 15$) M_{Jup} in logarithmic mass units, $N(M_1 \rightarrow M_2)/log(M_1/M_2)$, is large $\sim 10:1$ with an obviously large uncertainty due to the uncertain mass estimates. Kirkpatrick et al. (2012) cite a similar number, 6:1, from their volume limited brown dwarf sample. Evidently the star formation processes responsible for populating the local solar neighborhood did not produce large numbers of < 15 M_{Jup} objects. This same effect is seen in young clusters where the ratio of stars to brown dwarfs is more precisely estimated to be $\sim$ 6:1 (Anderson et al. 2008) and references therein.

It is interesting to note that objects with < 15 M_{Jup} appear to be difficult to create in the protostellar environments as well. Radial velocity studies find that massive objects are rare in the inner reaches of planetary systems with objects > 5 M_{Jup} accounting for fewer than 79 out of 882 or 9% presently cataloged planets within 10 AU of their host stars (Cumming et al. 2008; Howard et al. 2012). There are only 26 10 M_{Jup} objects out of 882 or just 3%. Here we have ignored the differences between M sin(i) and M which statistically reduces the number of low mass objects. Imaging surveys targeting the outer reaches of nearby A-F stars as well as lower mass M stars are beginning to either find objects of $\sim 5 - 10$ M_{Jup} or set limits on their occurrence. These coronagraphic studies are typically sensitive to 5-20 M_{Jup} objects with ages < 1 Gyr and located at orbital distances of tens to a few hundreds of AU. Apart from a dramatic examples like HR8799, Fomalhaut, and β Pictoris, the success rate of these surveys has been limited, typically a few percent. Around A stars Vigan et al. (2012) find the occurrence rate of a "planet" in the (3-14 M_{Jup}, 5-320 AU) range is $5.9 - 18\%$ (1σ), nominally a factor of two higher than the incidence of a "brown dwarf" in the (15-75 M_{Jup}, 5-320 AU) range. Nielsen et al. (2013) find the occurrence rate $< 20\%$ for (> 4 M_{Jup}, 59 and 460 AU) at 95% confidence, and <10% (> 10 M_{Jup}, 38 - 650 AU). They conclude by noting that "fewer than 10% of B and A stars can have an analog to the HR 8799 b (7 M_{Jup}, 68 AU) planet at 95% confidence." Around M stars, Montet et al. (2013) find an occurrence rate of $6.5 \pm 3.0\%$ for companions in the (1-13 M_{Jup}, 1-20 AU) range.

Imaging studies are in their infancy with significant advances in sensitivity and angular resolution coming in the next few years with the Gemini Planet Imager(Macintosh et al. 2012) and P1640 (Oppenheimer et al. 2012). The improvements in contrast and sensitivity will increase the completeness of imaging surveys in terms of their mass limit. Improvements in Inner Working Angle will increase survey completeness for as yet unexplored orbital separations and may thus find many more "super-Jupiters".

With these (uncertain) mass estimates in hand we can speculate as to the formation mechanism of these free floating planetary-mass objects. Observational evidence suggests at least two methods for brown dwarf formation: starlike formation from fragmentation of a molecular cloud (Bate et al. 2003, e.g.), possibly aided by turbulence (Padoan & Nordlund 2004), and protostellar disk fragmentation (Boss 2000; Stamatellos et al. 2007; Stamatellos & Whitworth 2009). Huard et al. (2006) and André et al. (2012) have both discovered proto-brown dwarf cores, indicating a starlike formation mechanism for at least some brown dwarfs. Young brown dwarfs have a similar disk fraction to young stars (Luhman et al. 2007) and show the same scaling between mass and accretion rate as stars, $\dot{M} \propto M^2$ (Muzerolle et al. 2003, 2005; Mohanty et al. 2005), again suggesting a common formation mechanism for stars and brown dwarfs. On the disk fragmentation side, Thies & Kroupa (2007) argue that there is a discontinuity in the IMF at the hydrogen-burning limit if unresolved binaries are taken into account, implying that brown dwarfs form differently from stars. Turbulent fragmentation has trouble explaining low-mass binaries: brown dwarf-brown dwarf pairs have not been observed in the numbers predicted (Reggiani & Meyer 2011), indicating that a different formation mechanism may be at work.

There are numerous reasons why both molecular cloud fragmentation and disk fragmentation produce fewer brown dwarfs than stars. While the opacity-limited minimum mass of fragments (either disk-born or cloud-born) is only 1–10 M_{Jup} (Low & Lynden-Bell 1976; Larson 2005; Whitworth & Stamatellos 2006), such fragments typically accrete mass and become stars (Bate et al. 2003; Kratter et al. 2010) given typical masses for molecular cloud cores and onset times for protostellar collapse (Myers 2009). Vorobyov (2013) argues that the probability of fragment survival in gravitationally unstable disks is low, as inward migration and subsequent ejection of fragments is efficient. Vorobyov also shows that fragment survival requires that the instability must happen in the T-Tauri phase of disk evolution rather than the embedded phase, yet the necessary conditions for T-Tauri disk fragmentation may occur only rarely. The median disk/star mass ratio of Class II YSOs inferred from dust continuum observations is only 0.9% (Andrews & Williams 2005, 2007). Even when gas is observed directly, as in the deuterated H_2 (HD) observations of TW Hydrae (Bergin et al. 2013), the masses inferred are almost always less than the $0.1 M_{disk}/M_*$ threshold required for disk fragmentation (Rafikov 2005).

If molecular cloud formation and disk fragmentation are both unlikely, it makes sense to consider whether core accretion—the planet formation process in which a solid core eventually grows large enough to hydrodynamically accrete gas from a disk—might form low-mass field brown dwarfs. Numerical simulations by Ford et al. (2001) show that 30% of the interactions between two giant planets near the stability boundary result in ejection, while microlensing measurements by Sumi et al. (2011) reveal a population of possibly unbound $1 M_{Jup}$ planetary-mass objects in the galactic bulge. Mordasini et al. (2012) find that the planet mass produced by core accretion falls off dramatically for $M > 3 M_{Jup}$ in disks with $M < 0.06 M_\odot$, which would explain the dearth of high-mass planets and field brown dwarfs. Yet Veras & Raymond (2012) argue that planet-planet scattering alone cannot explain the large number of unbound planets discovered by Sumi et al.,

who estimate two free-floating planets per solar-type star. Veras & Raymond instead suggest that other mechanisms for forming free floaters must be at work.

The likely formation mechanism for the free-floating objects presented here depends sensitively on their mass and velocity dispersion. In most cases the masses inferred from the BTSettl and Morley models are consistent with either disk fragmentation or starlike formation as most of the objects are above the rolloff in the planetary mass function predicted by Mordasini et al. (2012). For the lowest mass Y dwarfs such as WISE 1828+2650 ($\sim$5-10 M_{Jup}), core accretion followed by ejection from a planetary system might be the more favored mechanism as such low mass objects are at or below the opacity-limited minimum mass. However, core accretion near the star (where formation of a massive planet is favorable) followed by planet-planet scattering produces objects with a high velocity dispersion. Our objects have tangential velocities consistent with stars in the Solar neighborhood and inconsistent with an origin in nearby young clusters, i.e. $<$ 100 pc and $<$ 100 Myr (§ 5.2), implying that core accretion and ejection from a close-packed planetary system is unlikely. Both starlike formation and disk fragmentation followed by ejection of partially contracted clumps (Basu & Vorobyov 2012) both produce objects with low velocity dispersion, as observed for young brown dwarfs in Cha I(Joergens & Guenther 2001). Distinguishing between starlike formation and disk instability is difficult as both mechanisms are consistent with the observed IMF (Hennebelle & Chabrier 2009; Stamatellos & Whitworth 2009). In a review of brown dwarf observations to date, Luhman et al. (2007) conclude that starlike formation is the most likely origin for low-mass free floaters, while Bate (2012) argues that starlike formation, disk fragmentation, and ejection of collapsing cores from molecular clouds probably operate together. The existence of mass solutions that are typical for starlike formation or disk fragmentation, combined with the low velocity dispersion, suggests that our objects are brown dwarfs rather than free-floating planets.

6. Conclusions

We have carried out a program of imaging a selection of the coldest brown dwarfs detected by the WISE satellite, including 6 late T and and 9 Y dwarfs to obtain multi-epoch astrometry over a 2-3 year baseline. From these data we have determined parallax and proper motions with better than 15% accuracy for most of the sample with well determined distances ranging from 6 to 14 pc. By comparing absolute [4.5] magnitudes and a variety of colors from our Keck, HST and Spitzer photometry with models for low mass objects we can estimate masses and ages for this sample ranging between 3.4-8.8 Gyr and 12-30 M_{Jup} for the best fitting BT-Settl models. The fits for the coldest objects, e.g. WISE 1828+2650, are quite poor so these values remain highly uncertain. On the modeling side there is an urgent need for Y dwarf models with a broad range of metallicity, non-equilibrium chemistry, and effective temperatures as low as 300 K. Highly optically thick dust clouds ($A_V > 10$ mag) may be required to suppress the short wavelength emission and improve the agreement with the models. Observationally, it is critical to anchor these models with a few T or Y dwarf binaries for which dynamical masses can be obtained. In the future, long wavelength

photometry out to >10 μm with JWST will provide model-independent bolometric luminosities and effective temperatures. Moderate resolution spectroscopy from 1-10 μm will provide diagnostic spectral lines which can give much more precise information on physical conditions, especially surface gravity, than can broad band photometry.

Our parallaxes are similar to those estimated by other authors and confirm that local population of coldest brown dwarfs is sparse. The relative lack of brown dwarfs with masses below $\sim$15 M_{Jup} or exoplanets with masses above 10 M_{Jup} suggest this is a difficult mass range for the formation of objects in either environment. The dispersion in tangential velocities for our objects suggest that the objects detected by WISE are, however, likely to represent the lowest mass end of the star formation process rather than a population of objects formed by core accretion in a protoplanetary disk that we subsequently ejected (at high velocity) from their parent system.

The research described in this publication was carried out in part at the Jet Propulsion Laboratory, California Institute of Technology, under a contract with the National Aeronautics and Space Administration. This publication makes use of data products from the Wide-field Infrared Survey Explorer, which is a joint project of the University of California, Los Angeles, and the Jet Propulsion Laboratory/California Institute of Technology, funded by the National Aeronautics and Space Administration. This research has made use of the NASA/IPAC Infrared Science Archive (IRSA) and the NASA Exoplanet Archive which are operated by the Jet Propulsion Laboratory, California Institute of Technology, under contract with the National Aeronautics and Space Administration. This work is based in part on observations made with the *Spitzer* Space Telescope, which is operated by the Jet Propulsion Laboratory, California Institute of Technology, under a contract with NASA. This work is also based in part on observations made with the NASA/ESA *Hubble* Space Telescope, obtained at the Space Telescope Science Institute, which is operated by the Association of Universities for Research in Astronomy, Inc., under NASA contract NAS 5-26555. These observations are associated with program 12330. Support for program #12330 was provided by NASA through a grant from the Space Telescope Science Institute. Some data presented herein were obtained at the W. M. Keck Observatory from telescope time allocated to the National Aeronautics and Space Administration through the agency's scientific partnership with the California Institute of Technology and the University of California. The Observatory was made possible by the generous financial support of the W. M. Keck Foundation. The authors wish to recognize and acknowledge the very significant cultural role and reverence that the summit of Mauna Kea has always had within the indigenous Hawaiian community. We are most fortunate to have the opportunity to conduct observations from this mountain. The 2MASS catalog and the RECONS database of nearby stars remain invaluable resources. We acknowledge the assistance of Mr. Tahina Ramiaramanantsoa with the early stages of the reduction of these data and Ms. Dimitra Touli with the model fitting. Finally, we would like to thank the anonymous referee for a careful reading of our paper which led to a number of valuable improvements to both its content and presentation.

REFERENCES

Alcock, C., Allsman, R. A., Axelrod, T. S., et al. 1996, ApJ, 461, 84.

Alibert, Y., Mousis, O., Mordasini, C., & Benz, W. 2005, ApJ, 626, L57.

Allard, F., Guillot, T., Ludwig, H.-G., et al. 2003, Brown Dwarfs, 211, 325

Allard, F., Homeier, D., Freytag, B. 2010, *Proc. Cool Star XVI.*, p. 91.

Anderson, J., Sarajedini, A., Bedin, L. R., et al. 2008, AJ, 135, 2055.

André, P., Ward-Thompson, D., & Greaves, J. 2012, Science, 337, 69

Andrews, S. M., & Williams, J. P. 2005, ApJ, 631, 1134

Andrews, S. M., & Williams, J. P. 2007, ApJ, 671, 1800

Bahcall, J. N., & Casertano, S. 1985, ApJ, 293, L7.

Baraffe, I., Chabrier, G., Barman, T. S., Allard, F., & Hauschildt, P. H. 2003, A&A, 402, 701.

Basu, S., & Vorobyov, E. I. 2012, ApJ, 750, 30

Bate, M. R., Bonnell, I. A., & Bromm, V. 2003, MNRAS, 339, 577

Bate, M. R. 2012, MNRAS, 419, 3115

Becklin, E. E., & Neugebauer, G. 1967, ApJ, 147, 799.

Beichman, C. A., Myers, P. C., Emerson, J. P., et al. 1986, ApJ, 307, 337.

Beichman, C., Gelino, C. R., Kirkpatrick, J. D., et al. 2013, ApJ, 764, 101.

Bergin, E. A., Cleeves, L. I., Gorti, U., and 11 co-authors. 2013, Nature, 493, 644

Boss, A. P. 2000, ApJ, 536, L101.

Burningham, B., Cardoso, C. V., Smith, L., et al. 2013, MNRAS, 433, 457

Burrows, A., Marley, M., Hubbard, W. B., et al. 1997, ApJ, 491, 856.

Cumming, A., Butler, R. P., Marcy, G. W., et al. 2008, PASP, 120, 531

Cushing, M. C., Kirkpatrick, J. D., Gelino, C. R., et al. 2011, ApJ, 743, 50.

Cushing, M. C., Kirkpatrick, J. D., Gelino, C. R., et al. 2013, ApJ,submitted.

Cutri, R. M., Wright, E. L., Conrow, T., et al. 2011, *Explanatory Supplement to the WISE Preliminary Data Release Products.*

Dodson-Robinson, S. E., Veras, D., Ford, E. B.,& Beichman, C. A. 2009, ApJ, 707, 79.

Dunham, M. M., Arce, H. G., Allen, L. E., et al. 2013, AJ, 145, 94.

Dupuy, T. J., & Liu, M. C. 2012, ApJS, 201, 19.

Dupuy, T. J., & Kraus A. L. 2013, *Science*, in press, http://lanl.arxiv.org/pdf/1309.1422.pdf

Epchtein, N., de Batz, B., Capoani, L., et al. 1997, *The Messenger* , 87, 27.

Faherty, J. K., Burgasser, A. J., Cruz, K. L., et al. 2009, AJ, 137, 1.

Fazio, G. G., Hora, J. L., Allen, L. E., et al. 2004, ApJS, 154, 10.

Flynn, C., Gould, A., & Bahcall, J. N. 1996, ApJ, 466, L55.

Ford, E. B., Havlickova, M., & Rasio, F. A. 2001, Icarus, 150, 303

Green, R.M. 1985, *Spherical Astronomy* , Cambridge: Cambridge University Press, p.186.

Hennebelle, P., & Chabrier, G. 2009, ApJ, 702, 1428

Henry, T. J., Jao, W., Subasavage, J. P., et al. 2006, AJ, 132, 2360 (see also http://www.recons.org/census.posted.htm).

Howard, A. W., Marcy, G. W., Bryson, S. T., et al. 2012, ApJS, 201, 15

Huard, T. L., Myers, P. C., Murphy, D. C., et al. C. 2006, ApJ, 640, 391

Joergens, V., & Guenther, E. 2001, A&A, 379, 9

Kalas, P., Liu, M. C., & Matthews, B. C. 2004, Science, 303, 1990.

Kirkpatrick, J. D., Reid, I. N., Liebert, J., et al. 1999, ApJ, 519, 802.

Kirkpatrick, J. D. 2005, ARA&A, 43, 195.

Kirkpatrick, J. D., Cushing, M. C., Gelino, C. R., et al. 2011, ApJS, 197, 19.

Kirkpatrick, J. D., Gelino, C. R., Cushing, M. C., et al. 2012, ApJ, 753, 156

Kleinmann, D. E., & Low, F. J. 1967, ApJ, 149, L1.

Kozhurina-Platais, V., Cox, C., McLean, B., et al. 2009, Space Telescope WFC Instrument Science Report, 34.

Kratter, K. M., Murray-Clay, R. A., & Youdin, A. N. 2010, ApJ, 710, 1375

Lang, K.R. *Astrophysical Formulae: A Compendium for the Physicist and Astrophysicist* (Springer Study Edition), p. 262.

Larson, R. B. 1985, MNRAS, 214, 379.

Larson, R. B. 2005, MNRAS, 359, 211

Leggett, S. K., Saumon, D., Marley, M. S., et al. 2012, ApJ, 748, 74

Leggett, S. K., Morley, C. V., Marley, M. S., et al. 2013, ApJ, 763, 130.

Liu, M. C., Dupuy, T. J., Bowler, B. P., Leggett, S. K., & Best, W. M. J. 2012, ApJ, 758, 57.

Low, C., & Lynden-Bell, D. 1976, MNRAS, 176, 367.

Luhman, K. L., Joergens, V., Lada, C., et al. 2007, Protostars and Planets V, 443

Luhman, K. L., Burgasser, A. J., & Bochanski, J. J. 2011, ApJ, 730, L9.

Luhman, K. L., Burgasser, A. J., Labbé , I., et al. 2012, ApJ, 744, 135.

Lutz, T. E. & Kelker, D. H., PASP, 85, 573.

Mace, G. N., Kirkpatrick, J. D., Cushing, M. C., et al. 2013, ApJS, 205, 6.

Macintosh, B. A., Anthony, A., Atwood, J., et al. 2012, Proc. SPIE, 8446.

Mahmud, N., & Anderson, J. 2008, PASP, 120, 907.

Marley, M. S., Fortney, J. J., Hubickyj, O., Bodenheimer, P., & Lissauer, J. J. 2007, ApJ, 655, 541.

Marley, M. S., Saumon, D., & Goldblatt, C. 2010, ApJ, 723, L117.

Marois, C., Macintosh, B., Barman, T., et al. 2008, Science, 322, 1348.

Marsh, K. A., Wright, E. L., Kirkpatrick, J. D., et al. 2013, ApJ, 762, 119.

Mohanty, S., Jaywardhana, R., & Basri, G. 2005, ApJ, 626, 498

Monet, D. G., Jenkins, J. M., Dunham, E. W., et al. 2010, arXiv:1001.0305.

Montet, B. et al. 2013, submitted to ApJ, http://arxiv.org/abs/1307.5849.

Mordasini, C., Alibert, Y., Klahr, H., & Henning, T. 2012, A&A, 547, A111

Morley, C. V., Fortney, J. J., Marley, M. S., et al. 2012, ApJ, 756, 172.

Muzerolle, J., Hillenbrand, L., Calvet, N., Briceño, C., & Hartmann, L. 2003, ApJ, 592, 266

Muzerolle, J., Luhman, K. L., Briceño, C., Hartmann, L., & Calvet, N. 2005, ApJ, 625, 906

Myers, P. C. 2009, ApJ, 706, 1341

Nakajima, T., Oppenheimer, B. R., Kulkarni, S. R., et al. 1995, Nature, 378, 463.

Nielsen, E. L., Liu, M. C., Wahhaj, Z., et al. 2013, arXiv:1306.1233.

Oppenheimer, B. R., Beichman, C., Brenner, D., et al. 2012, Proc. SPIE, 8447,

Padoan, P., & Nordlun, A. 2004, ApJ, 617, 559

Rafikov, R. R. 2005, ApJ, 621, 69

Rajan, A. et al. 2010, WFC3 Data Handbook, Version 2.1, (Baltimore: STScI).

Reggiani, M. M., & Meyer, M. R. 2011, ApJ, 738, 60

Saumon, D., & Marley, M. S. 2008, ApJ, 689, 1327.

Schmidt, M. 1968, ApJ, 151, 393.

Shu, F. H., Adams, F. C., & Lizano, S. 1987, ARA&A, 25, 23.

Skrutskie, M. F., Cutri, R. M., Stiening, R., et al. 2006, AJ, 131, 1163.

Smart, W.M. *Textbook on Spherical Astronomy, 6^{th} Ed.* , Cambridge, UK:Cambridge Univ Press, p. 221.

Stamatellos, D., Hubber, D. A., & Whitworth, A. P. 2007, MNRAS, 382, L30

Stamatellos, D., & Whitworth, A. P. 2009, MNRAS, 392, 413

Stone, R. C. 1996, PASP, 108, 1051.

Sumi, T., Kamiya, K., Bennett, D. P., et al. 2011, Nature, 473, 349.

Thies, I., & Kroupa, P. 2007, ApJ, 671, 767

van Dam, M. A., et al. 2006, PASP, 118, 310.

Veras, D., & Raymond, S. N. 2012, MNRAS, 421, 117

Vigan, A., Patience, J., Marois, C., et al. 2012, A&A, 544, A9.

Vorobyov, E. 2013, A&A, 552, 129

Whitworth, A. P., & Stamatellos, D. 2006, A&A, 458, 817

Wizinowich, P. L., et al. 2006, PASP, 118, 297.

Wright, E. L., Eisenhardt, P. R. M., Mainzer, A. K., et al. 2010, AJ, 140, 1868

York, D. G., Adelman, J., Anderson, J. E., Jr., et al. 2000, AJ, 120, 1579.

Wilson, R. W., Jefferts, K. B., & Penzias, A. A. 1970, ApJ, 161, L43.

Zuckerman, B., & Song, I. 2004, ARA&A, 42, 685

This preprint was prepared with the AAS LaTeX macros v5.2.

Table 1. Astrometric Targets

WISE Designation	Spectral Type	Sp. Ref	Detections (M/N)[a]	# Keck Obs.	# Hubble Obs.	# Spitzer Obs.	Baseline (yr)
J014656.66+423410.0 (WISE0146+42)	Y0	1	13/39	7	0	8	2.5
J031325.94+780744.2 (WISE0313+78)	T8.5	3	16/16	4	0	5	3.6
J033515.01+431045.1 (WISE0335+43)	T9	4	9/12	5	1	8	2.4
J041022.71+150248.4[b] (WISE0410+15)	Y0	2	12/12	2	1	11	2.3
J071322.55-291751.9 (WISE0713-29)	Y0	1	11/15	5	0	5	1.3
J083641.10-185947.0 (WISE0836-18)	T8p	3	7/15	4	0	3	2.1
J131106.20+012254.3 (WISE1311+01)	T9:	3	9/17	5	0	4	2.2
J154151.65-225024.9 (WISE1541-22)	Y0.5	2	10/10	4	2	4	2.1
J154214.00+223005.2 (WISE1542+22)	T9.5	4	22/45	1	2	3	1.8
J173835.53+273259.0[b] (WISE1738+27)	Y0	2	16/18	3	1	10	2.7
J180435.37+311706.4 (WISE1804+31)	T9.5:	3	15/19	5	0	9	3.0
J182831.08+265037.7[b] (WISE1828+26)	$\geq$Y2	1	12/18	5	4	11	2.9
J205628.91+145953.2 (WISE2056+14)	Y0	2	12/12	6	1	11	2.9
J220905.73+271143.9 (WISE2209+27)	Y1	5	13/15	4	1	6	2.4
J222055.31-362817.4 (WISE2220-36)	Y0	1	11/17	2	1	6	1.8

Note. — [a]Number of *actual* detections, M, relative to number of *possible* detections, N in WISE W2 band. [1]Kirkpatrick et al. (2012); [2]Cushing et al. (2011);[3]Kirkpatrick et al. (2011);[4]Mace et al. (2013);[5]Cushing et al. (2013)

Table 2. Observing Log and Astrometric Data

WISE Designation	Observatory	Date (UT)	Filter	AOR	PI	MJD	RA (J2000)	DEC (J2000)	Uncertainty (mas)
J014656.66+423410.0	WISE	2010-Jan-27				55223.14	26.7361144	42.5694586	250
	Spitzer	2011-Apr-05	Ch1	41808128	Kirkpatrick	55656.09	26.7359654	42.5694282	60
	Spitzer	2011-Apr-05	Ch2	41808128	Kirkpatrick	55656.09	26.7359584	42.5693949	60
	Keck	2011-Dec-19	H		Beichman	55914.28	26.7358852	42.5694054	50
	Spitzer	2012-Mar-07	H		Beichman	55993.04	26.7358141	42.5694177	60
	Spitzer	2012-Mar-07	Ch2	44544000	Kirkpatrick	55993.04	26.7358141	42.5694177	60
	Spitzer	2012-Oct-15	Ch2	44588544	Kirkpatrick	56215.07	26.7358141	42.5694177	50
	Keck	2013-Jan-25	H		Beichman	56317.22	26.7356976	42.5694103	30
	Spitzer	2013-Mar-13	H		Beichman	56364.25	26.7356437	42.5693903	60
	Spitzer	2013-Mar-13	Ch2	46549760	Kirkpatrick	56364.25	26.7356437	42.5693903	60
	Spitzer	2013-Mar-21	Ch2	46549504	Kirkpatrick	56372.31	26.7356303	42.5694013	60
	Spitzer	2013-Apr-06	Ch2	46549248	Kirkpatrick	56388.81	26.7356659	42.5693978	60
	Spitzer	2013-Apr-11	Ch2	46548992	Kirkpatrick	56393.13	26.7356847	42.5693894	60
	Keck	2013-Sep-20	H		Beichman	56555.42	26.7356234	42.5694212	20
	Keck	2013-Nov-19	H		Beichman	56615.29	26.7355696	42.569411	30
J031358.93+780748.9	WISE	2010-Dec-21				55256.99	48.3581137	78.1289762	250
	WISE	2010-Dec-21				55448.08	48.35846	78.1289878	250
	Spitzer	2010-Dec-21	Ch1	41443840	Kirkpatrick	55551.35	48.3586706	78.1290368	60
	Spitzer	2010-Dec-21	Ch2	41443840	Kirkpatrick	55551.35	48.3586761	78.1290121	60
	Spitzer	2011-Apr-23	Ch2	41735936	Kirkpatrick	55674.71	48.3584757	78.128978	60
	Keck	2011-Oct-16	H		Beichman	55850.57	48.3588985	78.1290222	20
	Spitzer	2011-Dec-02	Ch2	44803072	Kirkpatrick	55897.22	48.3588009	78.1290122	60
	Spitzer	2012-Apr-24	Ch2	44798464	Kirkpatrick	56041.15	48.3585303	78.1290161	60
	Keck	2012-Oct-07	H		Beichman	56207.51	48.3589982	78.1290526	20
	Keck	2013-Jan-25	H		Beichman	56317.25	48.3587497	78.1290253	30
	Keck	2013-Sep-20	H		Beichman	56555.53	48.3591015	78.129052	30
J033515.01+431045.1	WISE1	2010-Feb-15				55242.16	53.8125634	43.1791225	310
	WISE2	2010-Aug-27				55435.86	53.8127677	43.1791506	150
	Spitzer	2011-Apr-19	Ch1	41838848	Kirkpatrick	55670.15	53.8129519	43.1789742	60
	Spitzer	2011-Apr-19	Ch2	41838848	Kirkpatrick	55670.15	53.8129111	43.1789762	60
	Spitzer	2011-Nov-17	Ch2	44573696	Kirkpatrick	55882.78	53.8131682	43.1788608	60
	Keck	2012-Oct-07	H		Beichman	56207.59	53.8134114	43.17867	20
	Spitzer	2012-Nov-22	Ch2	46436096	Kirkpatrick	56253.19	53.8134568	43.1786443	60
	Keck	2012-Nov-29	H		Beichman	56260.38	53.8134285	43.1786345	20
	Keck	2013-Jan-25	H		Beichman	56317.32	53.8134738	43.1785834	20
	HST	2013-Mar-29	F125W		Cushing	56380.74	53.8135311	43.1785361	20
	Spitzer	2013-Apr-07	Ch2	46595328	Kirkpatrick	56389.02	53.8135567	43.178527	60
	Spitzer	2013-Apr-17	Ch2	46595072	Kirkpatrick	56399.8	53.8135846	43.1785371	60
	Spitzer	2013-Apr-22	Ch2	46594816	Kirkpatrick	56404.5	53.8135702	43.1785451	60
	Spitzer	2013-May-05	Ch2	46594560	Kirkpatrick	56417.21	53.8135371	43.1785424	60
	Keck	2013-Sep-20	H		Beichman	56555.56	53.813732	43.1784515	20
	Keck	2013-Nov-19	H		Beichman	56615.32	53.813756	43.1784148	20
J041022.71+150248.4	WISE	2010-Feb-16				55243.6	62.5946547	15.046819	250
	WISE	2010-Aug-26				55434.09	62.594941	15.0464875	250
	Spitzer	2010-Oct-21	Ch1	40828160	Kirkpatrick	55490.06	62.5949777	15.0464452	55
	Spitzer	2010-Oct-21	Ch2	40828160	Kirkpatrick	55490.06	62.5949953	15.0464292	55
	Spitzer	2011-Apr-14	Ch2	41442304	Kirkpatrick	55665.88	62.5950177	15.0460896	55
	HST	2012-Sep-01	F140W		Cushing	56171.83	62.5954954	15.0452734	20
	Spitzer	2011-Nov-19	Ch2	44567808	Kirkpatrick	55884.56	62.5952786	15.0457531	55
	Spitzer	2011-Nov-24	Ch1	44508160	Dupuy	55889.76	62.5952814	15.0457285	55
	Spitzer	2012-Mar-29	Ch1	44508416	Dupuy	56015.06	62.5952928	15.0455135	55
	Spitzer	2012-Mar-30	Ch2	44564480	Kirkpatrick	56016.76	62.5952956	15.0455307	55
	Spitzer	2012-Apr-29	Ch1	44508672	Dupuy	56046.9	62.5953018	15.0454548	55
	Spitzer	2012-Oct-30	Ch1	44508672	Dupuy	56230.96	62.5955446	15.0451638	55
	Spitzer0	2012-Nov-19	Ch2	46443008	Kirkpatrick	56250.9	62.595579	15.0451303	55
	Spitzer1	2012-Nov-30	Ch2	46442752	Kirkpatrick	56261.93	62.5955494	15.0451248	55
	Keck	2013-Jan-25	H		Beichman	56317.28	62.5955394	15.0450125	40
	Keck	2013-Feb-20	H		Beichman	56343.24	62.5955423	15.0449683	20
J071322.55-291751.9	WISE	2010-Apr-09				55296.64	108.3439684	-29.2977331	160
	WISE	2010-Oct-18				55488.21	108.3441041	-29.2978282	200
	Keck	2011-Oct-16	H		Beichman	55850.64	108.3442071	-29.2979174	30
	Spitzer	2012-Jan-02	Ch1	44568064	Kirkpatrick	55928.89	108.344187	-29.2979651	80
	Spitzer	2012-Jan-02	Ch2	44568064	Kirkpatrick	55928.89	108.3442477	-29.2979653	55
	Keck	2012-Mar-31	H		Beichman	56017.24	108.3441896	-29.2979665	30
	Keck	2012-Oct-07	H		Beichman	56207.63	108.3443149	-29.2980289	30
	Spitzer	2012-Dec-25	Ch2	46439936	Kirkpatrick	56286.71	108.3443274	-29.2980777	55
	Spitzer	2013-Jan-17	Ch2	46439680	Kirkpatrick	56309.98	108.3443808	-29.2980687	55

Table 2—Continued

WISE Designation	Observatory	Date (UT)	Filter	AOR	PI	MJD	RA (J2000)	DEC (J2000)	Uncertainty (mas)
	Keck	2013-Jan-25	H		Beichman	56317.35	108.3443186	-29.2980846	20
	Spitzer	2013-Feb-06	Ch2	46439424	Kirkpatrick	56329.14	108.3443683	-29.2981035	55
	Keck	2013-Feb-20	H		Beichman	56343.28	108.3443092	-29.2980885	30
J083641.10-185947.0	WISE	2010-May-02				55319.67	129.1712834	-18.9963895	1000
	WISE	2010-Nov-10				55510.55	129.1714539	-18.996376	1220
	Spitzer	2011-Jan-01	Ch2	40833536	Kirkpatrick	55563	129.1715552	-18.9962973	50
	Spitzer	2011-May-31	Ch2	41701888	Kirkpatrick	55712.03	129.1715494	-18.9963169	50
	Spitzer	2012-Jan-17	Ch2	44556032	Kirkpatrick	55943.76	129.1715477	-18.9963443	50
	Keck	2012-Nov-29	H		Beichman	56260.57	129.1715439	-18.9963665	30
	Keck	2013-Jan-25	H		Beichman	56317.41	129.17153	-18.9963856	20
	Keck	2013-Feb-20	H		Beichman	56343.33	129.1715283	-18.9963813	20
	Keck	2013-Nov-19	H		Beichman	56615.59	129.1715276	-18.996414	20
J131106.20+012254.3	WISE	2010-Jan-09				55206.33	197.7760137	1.3817997	350
	WISE	2010-Jul-02				55380.12	197.7759224	1.3817217	340
	Spitzer	2011-Mar-29	Ch1	40826368	Kirkpatrick	55649.37	197.7761222	1.3814907	60
	Spitzer	2011-Mar-29	Ch2	40826368	Kirkpatrick	55649.37	197.7760981	1.3815201	60
	Spitzer	2012-Mar-29	Ch2	44575232	Kirkpatrick	56015.51	197.7762172	1.3812636	60
	Keck	2012-Mar-31	H		Beichman	56017.4	197.7761705	1.3812709	30
	Keck	2012-Jul-09	H		Beichman	56117.26	197.7761937	1.3812213	30
	Spitzer	41143	Ch2	44571904	Kirkpatrick	56161.13	197.7761852	1.3811918	50
	Keck	2013-Jan-25	H		Beichman	56317.5	197.7762561	1.3810702	30
	Keck	2013-Feb-20	H		Beichman	56343.45	197.776254	1.3810576	20
	Keck	2013-May-27	H		Beichman	56439.25	197.7762548	1.3810158	20
J154151.65-225024.9	WISE	2010-Feb-16				55244.84	235.4651965	-22.840523	500
	Spitzer	2011-Apr-13	Ch1	41788672	Kirkpatrick	55664.91	235.4648435	-22.8404433	66
	Spitzer	2011-Apr-13	Ch2	41788672	Kirkpatrick	55664.91	235.4648328	-22.8404443	60
	WISE	2010-Aug-15				55424	235.4650457	-22.8400781	500
	Spitzer	2012-Apr-22	Ch1	44512512	Dupuy	56039.24	235.4645941	-22.8404542	80
	Spitzer	2012-Apr-28	Ch2	44550144	Kirkpatrick	56045.83	235.4646137	-22.840462	60
	Keck	2012-Mar-31	H		Beichman	56017.51	235.464582	-22.840456	20
	Spitzer	2012-May-19	Ch1	44512768	Dupuy	56066.22	235.464575	-22.8404522	85
	Keck	2012-Jul-09	H		Beichman	56117.28	235.464431	-22.840446	20
	Keck	2013-Jan-25	H		Beichman	56317.63	235.4643821	-22.840476	20
	HST	2013-Feb-12	F125W		Cushing	56335.74	235.4643635	-22.8404761	20
	HST	2013-May-09	F105W		Cushing	56421.55	235.4642595	-22.8404771	20
	Keck	2013-May-27	H		Beichman	56439.33	235.4642458	-22.8404802	20
J154214.00+223005.2	WISE	2010-Feb-04				55232.37	235.558604	22.5015172	400
	WISE	2010-Aug-03				55412.02	235.5583999	22.5015432	400
	Spitzer	2011-Apr-18	Ch1	41058816	Kirkpatrick	55669.41	235.5579949	22.5013517	60
	Spitzer	2011-Apr-18	Ch2	41058816	Kirkpatrick	55669.41	235.5580421	22.5013728	60
	Spitzer	2012-Apr-15	Ch2	44559616	Kirkpatrick	56032.02	235.5577765	22.5012418	60
	HST	2012-Mar-04	F140W		Kirkpatrick	55990.91	235.5577799	22.5012605	15
	Spitzer	2012-Sep-21	Ch2	44557568	Kirkpatrick	56191.18	235.5575565	22.5012083	60
	HST	2013-Feb-13	F125W		Cushing	56336.82	235.557504	22.5011602	15
	Keck	2013-Feb-20	H		Beichman	56343.52	235.5575356	22.5011738	60
J173835.53+273259.0	WISE	2010-Mar-13				55269.03	264.6480543	27.5496933	250
	Spitzer	2010-Sep-18	Ch1	40828416	Kirkpatrick	55457.58	264.6480843	27.549658	50
	Spitzer	2010-Sep-18	Ch2	40828416	Kirkpatrick	55457.58	264.6480788	27.5496439	50
	WISE	2010-Sep-09				55448.65	264.6481684	27.5496833	250
	HST	2011-May-12	F140W		Kirkpatick	55693.81	264.6481914	27.5495878	15
	Spitzer	2011-May-20	Ch2	41515264	Kirkpatrick	55701.63	264.6482049	27.549556	50
	Spitzer	2011-Nov-26	Ch2	41515264	Kirkpatrick	55891.28	264.648178	27.5495077	50
	Keck	2012-Mar-31	H		Beichman	56017.55	264.6482856	27.5495029	25
	Spitzer	2012-May-08	Ch1	44513536	Dupuy	56055.9	264.6482997	27.549458	50
	Spitzer	2012-May-12	Ch2	44558336	Kirkpatrick	56059.9	264.6483229	27.5494919	50
	Keck	2012-Jul-09	H		Beichman	56117.26	264.6482643	27.5495025	30
	Spitzer	2012-Jul-10	Ch1	44513792	Dupuy	56118.85	264.6483209	27.5494664	50
	Spitzer	2012-Sep-27	Ch1	44513024	Dupuy	56197.4	264.6482847	27.5494635	50
	Spitzer	2012-Nov-19	Ch2	46437888	Kirkpatrick	56250.73	264.6482591	27.5494299	50
	Spitzer	2012-Nov-27	Ch1	44513280	Dupuy	56258.77	264.6482799	27.5494348	50
	Keck	2013-May-27	H		Beichman	56439.43	264.6483932	27.5494055	30
J180435.37+311706.4	WISE	2010-Mar-21				55277.1	271.1472306	31.2851638	340
	WISE	2010-Nov-09				55509.91	271.1471832	31.2852385	280
	Spitzer	2010-Sep-26	Ch1	40836352	Kirkpatrick	55465.2	271.1472408	31.2851226	50
	Spitzer	2010-Sep-26	Ch2	40836352	Kirkpatrick	55465.2	271.1472431	31.2851484	50
	Spitzer	2011-May-25	Ch2	41565696	Kirkpatrick	55706.84	271.1472367	31.2851427	50
	Spitzer	2011-Nov-29	Ch2	44571136	Kirkpatrick	55894.05	271.14717	31.2851347	50

Table 2—Continued

WISE Designation	Observatory	Date (UT)	Filter	AOR	PI	MJD	RA (J2000)	DEC (J2000)	Uncertainty (mas)
	Keck	2012-Jul-09	H		Beichman	56117.37	271.1470991	31.2851768	30
	Spitzer	2011-Dec-01	Ch1	44515328	Dupuy	55896.97	271.1471423	31.2851566	50
	Spitzer	2012-May-16	Ch1	44515584	Dupuy	56063.73	271.147159	31.2851443	50
	Spitzer	2012-May-16	Ch2	44515584	Dupuy	56063.75	271.1471621	31.2851558	50
	Spitzer	2012-Jul-25	Ch1	44515840	Dupuy	56133.39	271.1471254	31.2851738	50
	Spitzer	2012-Oct-03	Ch1	44515072	Dupuy	56203.43	271.1470927	31.2851711	50
	Keck	2013-Apr-22	H		Beichman	56404.53	271.1470676	31.2851603	20
	Keck	2013-May-27	H		Beichman	56439.4	271.147049	31.2851677	20
J182831.08+265037.7	WISE1	2010-Mar-30				55285.66	277.1295162	26.8438	170
	WISE	2010-Sep-28				55467.55	277.1295247	26.8439192	210
	Keck	2010-Jul-01	H		Beichman	55378.44	277.1296241	26.8438953	100
	Spitzer	2010-Jul-10	Ch1	39526656	Mainzer	55387.29	277.1296029	26.8438554	60
	Spitzer	2010-Jul-10	Ch2	39526656	Mainzer	55387.34	277.1296042	26.8438808	60
	Spitzer	2010-Dec-04	Ch2	41027328	Kirkpatrick	55534.27	277.1296675	26.8438286	60
	HST	2011-May-09	F140W		Kirkpatrick	55690.89	277.1298806	26.8439048	30
	Keck	2011-Oct-16	H		Beichman	55850.21	277.1299543	26.8439071	10
	Spitzer	2011-Nov-29	Ch2	44586752	Kirkpatrick	55894.04	277.1300176	26.8438958	60
	Spitzer	2011-Dec-02	Ch1	44516352	Dupuy	55897.48	277.1300065	26.8439088	60
	Spitzer	2012-May-25	Ch1	44516608	Dupuy	56072.2	277.1302159	26.8439439	60
	Spitzer	2012-May-25	Ch2	44516608	Dupuy	56072.25	277.1301923	26.8439382	60
	Keck	2012-Jul-09	H		Beichman	56117.32	277.1302146	26.8439617	10
	Spitzer	2012-Jul-23	Ch1	44516864	Dupuy	56131.04	277.1302484	26.8439671	60
	Keck	2012-Oct-07	H		Beichman	56207.22	277.1302611	26.8439344	50
	Spitzer	2012-Oct-18	Ch2	44516096	Dupuy	56218.2	277.1302737	26.84398	60
	Spitzer0	2012-Nov-18	Ch2	46439168	Kirkpatrick	56249.43	277.1302789	26.8439821	60
	Spitzer1	2012-Dec-08	Ch2	46438912	Kirkpatrick	56269.92	277.1303385	26.8439822	60
	HST	2013-Apr-22	F105W		Cushing	56404.88	277.1305007	26.8439937	10
	HST	2013-May-06	F125W		Cushing	56418.83	277.1305121	26.844001	10
	HST	2013-May-08	F105W		Cushing	56420.76	277.13051	26.8440029	10
	Keck	2013-May-27	H		Beichman	56439.36	277.1305206	26.8440076	10
J205628.91+145953.2	WISE-1	2010-May-13				55329.29	314.1204976	14.9981178	290
	Keck	2010-Jul-01	H		Beichman	55378.6	314.1204617	14.9981905	30
	WISE	2010-Nov-08				55514.2	314.1204976	14.9981178	290
	Spitzer	2010-Dec-10	Ch1	40836608	Kirkpatrick	55540.03	314.1205267	14.9982425	60
	Spitzer	2010-Dec-10	Ch2	40836608	Kirkpatrick	55540.03	314.1205241	14.998241	60
	Spitzer	2011-Jul-06	Ch2	41831424	Kirkpatrick	55748.1	314.1207526	14.9983505	60
	HST	2011-Sep-05	F140W		Kirkpatrick	55808.36	314.1207034	14.9983548	20
	Keck	2011-Oct-16	H		Beichman	55850.35	314.1207055	14.9983614	20
	Keck	2011-Dec-19	H		Beichman	55914.2	314.1207544	14.9983705	40
	Spitzer	2012-Jan-06	Ch2	44573184	Kirkpatrick	55932.56	314.1207682	14.998396	60
	Spitzer	2012-Jan-22	Ch1	44517376	Dupuy	55948.98	314.1207601	14.9983875	60
	Keck	2012-Jul-09	H		Beichman	56117.46	314.1209349	14.9984907	20
	Spitzer	2012-Jul-10	Ch1	44517632	Dupuy	56118.83	314.1209268	14.9984825	60
	Keck	2012-Oct-07	H		Beichman	56207.28	314.120941	14.9985341	50
	Spitzer	2012-Jul-18	Ch2	44569600	Kirkpatrick	56126.76	314.1209601	14.9984791	60
	Spitzer	2012-Aug-21	Ch1	44517888	Dupuy	56160.05	314.1209851	14.9984985	60
	Spitzer	2012-Dec-22	Ch2	46464000	Kirkpatrick	56283.4	314.1209624	14.9985174	60
	Spitzer	2013-Jan-04	Ch2	46463488	Kirkpatrick	56296.19	314.1210188	14.9985212	60
	Spitzer	2013-Jan-22	Ch2	46462720	Kirkpatrick	56314.75	314.1210053	14.9985509	60
	Keck	2013-May-27	H		Beichman	56439.46	314.1211613	14.998618	20
J220905.73+271143.9	WISE	2010-Jun-06				55354.86	332.2739012	27.1955919	250
	Spitzer	2010-Dec-31	Ch2	40821248	Kirkpatrick	55561.94	332.2740681	27.1953371	60
	Keck	2011-Jul-20	H		Beichman	55762.5	332.2743368	27.1951698	30
	Spitzer	2011-Jul-27	Ch2	41698816	Kirkpatrick	55769.86	332.2743509	27.1951224	60
	Spitzer	2012-Jan-14	Ch2	44548352	Kirkpatrick	55940.6	332.2744675	27.1949265	60
	Keck	2012-Jul-09	H		Beichman	56117.52	332.2747063	27.1948078	30
	Keck	2012-Oct-07	H		Beichman	56207.32	332.2747329	27.1946743	30
	HST	2012-Sep-15	F140W		Cushing	56185.58	332.2747399	27.1947115	20
	Spitzer	2013-Jan-10	Ch2	46543616	Kirkpatrick	56302.15	332.2748377	27.1945693	60
	Spitzer	2013-Jan-31	Ch2	46543360	Kirkpatrick	56323.38	332.2748291	27.1945492	60
	Spitzer	2013-Feb-14	Ch2	46543104	Kirkpatrick	56337.87	332.2748893	27.1945119	60
	Keck	2013-May-27	H		Beichman	56439.53	332.2750607	27.1944435	20
J222055.31-362817.4	WISE	2010-May-14				55330.96	335.2304846	-36.4713796	332
	WISE	2010-Nov-09				55509.91	335.23058743	-36.4715195	281
	Spitzer	2012-Jan-23	Ch1	44552448	Kirkpatrick	55949.11	335.23056511	-36.4715078	60
	Spitzer	2012-Jan-23	Ch2	44552448	Kirkpatrick	55949.11	335.23056635	-36.4715455	60
	Spitzer	2012-Jul-15	Ch2	44574464	Kirkpatrick	56123.9	335.23068028	-36.4715003	60

Table 2—Continued

WISE Designation	Observatory	Date (UT)	Filter	AOR	PI	MJD	RA (J2000)	DEC (J2000)	Uncertainty (mas)
	HST	2012-Nov-23	F125W		Cushing	56254.33	335.23066052	-36.4715666	20
	Spitzer	2012-Dec-24	Ch2	46460928	Kirkpatrick	56285.09	335.23068603	-36.471558	60
	Spitzer	2013-Jan-06	Ch2	46460160	Kirkpatrick	56298.03	335.23065602	-36.4715587	60
	Spitzer	2013-Jan-26	Ch2	46459392	Kirkpatrick	56318.93	335.2307343	-36.4715553	60
	Keck	2013-Sep-21	H		Beichman	56556.32	335.23076402	-36.4715891	10
	Keck	2013-Nov-19	H		Beichman	56615.2	335.2307524	-36.4715821	10

Table 3. Photometric Data (Magnitudes)

WISE Designation	F105W	J	F125W	F140W	H[a]	WISE [3.35]	Spitzer [3.6]	Spitzer [4.5]	WISE [4.6]
J014656.66+423410.0		19.40±0.25[b]			20.91±0.21	>18.99	17.42±0.05	15.05±0.03	15.08±0.068
J031325.94+780744.2		17.67±0.07[b]			17.67±0.07	15.87±0.058	15.31±0.05	13.23±0.03	13.18±0.03
J033515.01+431045.1		20.07±0.30[d]	20.23±0.05		19.76±0.13	>18.15	16.58±0.05	14.39±0.03	14.60±0.08
J041022.71+150248.4		19.44±0.03[e]		19.74±0.03	20.02±0.05[e]	>18.25	16.62±0.05	14.10±0.03	14.18±0.055
J071322.55-291751.9		19.64±0.15[b]			19.85±0.05	>18.35	16.67±0.05	14.22±0.03	14.48±0.06
J083641.10-185947.0		18.99±0.22[d]			19.49±0.24	>18.41	16.85±0.05	15.06±0.03	15.18±0.098
J131106.20+012254.3		18.75±0.07[c]			19.09±0.07	>18.27	16.81±0.05	14.64±0.03	14.76±0.086
J154151.65-225024.9	21.41±0.01	21.12±0.06[e]	21.69±0.05		21.54±0.11	16.74±0.16	16.70±0.05	14.21±0.03	14.26±0.06
J154214.00+223005.2		20.25±0.13[d]	20.73±0.03	20.46±0.03	20.34±0.06	>18.88	17.27±0.05	15.02±0.03	15.02±0.06
J173835.53+273259.0		20.05±0.09[e]		19.89±0.05	20.45±0.09[e]	>18.40	16.94±0.05	14.49±0.03	14.55±0.06
J180435.37+311706.4		18.67±0.04[f]			19.21±0.11[b]	>18.64	16.55±0.05	14.59±0.03	14.74±0.06
J182831.08+265037.7	23.96±0.10	23.57±0.35[g]	23.83±0.05	23.36±0.05	22.45±0.08[g]	>18.47	16.88±0.05	14.30±0.03	14.39±0.06
J205628.91+145953.2		19.43±0.04[e]		19.57±0.04	19.96±0.04[e]	>18.25	16.07±0.05	13.92±0.03	13.98±0.05
J220905.73+271143.9		22.58±0.14[h]		23.17±0.03	22.98±0.31[h]	>18.47	N/A	14.71±0.03	14.79±0.07
J222055.31-362817.4		20.38±0.17[b]	21.21±0.05		20.81±0.30[b]	>18.65	17.17±0.05	14.75±0.03	14.66±0.06

Note. — [a]Unless otherwise noted, H-band photometry is from NIRC2 from observations reported here. Photometry is on the MKO-NIR system; [b]Kirkpatrick et al. (2012); [c]Kirkpatrick et al. (2011); [d]Mace et al. (2013); [e]Leggett et al. (2013); [f]unpublished Palomar WIRC data; [g]Beichman et al. (2013); [h]Cushing et al. (2013).

Table 4. Spitzer Photometric Variability (Channel 2)

WISE Designation	# Observations	σ_{pop} (mag)
J014656.66+423410.0	7	0.013
J031325.94+780744.2	4	0.030
J033515.01+431045.1	7	0.012
J041022.71+150248.4	9	0.030
J071322.55-291751.9	4	0.007
J083641.10-185947.0	3	0.007
J131106.20+012254.3	3	0.010
J154151.65-225024.9	2	<0.1[a]
J154214.00+223005.2	3	0.017
J173835.53+273259.0	5	0.024
J180435.37+311706.4	4	0.006
J182831.08+265037.7	6	0.013
J205628.91+145953.2	7	0.015
J220905.73+271143.9	6	0.019
J222055.31-362817.4	5	0.020

Note. — [a]Confused with nearby star

Table 5. Astrometric Reference Frames

WISE Designation	N[1]	σ(Ref,mas)[2]	σ(Limit,mas)[3]	N[4]	σ(Ref,mas)[5]	N[6]	σ(Ref,mas)[7]	σ(Theta,deg)[8]
		Spitzer		**HST-Spitzer**		**Spitzer/HST-Keck**		
J014656.66+423410.0	98	1	59	N/A	N/A	3	5-30	0.04-0.16
J031325.94+780744.2	103	2.5	56	N/A	N/A	4	6-28	0.044-0.066
J033515.01+431045.1	141	0.8	60	11	19	10	14-19	0.011-0.017
J041022.71+150248.4	63	0.3	55	9	24	5	10-30	0.02-0.08
J071322.55-291751.9	73	1.5	53	N/A	N/A	6	16-20	0.015-0.022
J083641.10-185947.0	46	2.3	47	N/A	N/A	5	27-29	0.06-0.12
J131106.20+012254.3	27	1.2	42	N/A	N/A	5	14-28	0.03-0.06
J154151.65-225024.9	107	0.5	47	10	5	7-10	8-17	0.007-0.022
J154214.00+223005.2	81	0.8	63	10	14	3	30	0.11
J173835.53+273259.0	28	0.5	54	N/A	N/A	6	10-20	0.011-0.018
J180435.37+311706.4	102	0.5	55	N/A	N/A	8	14-17	0.011-0.015
J182831.08+265037.7	27	1.5	48	16	5-15	9-10	4-15	0.003-0.018
J205628.91+145953.2	134	3	75	12	10	6-7	5-18	0.007-0.038
J220905.73+271143.9	105	0.5	62	10	9	5-8	5-22	0.021-0.045
J222055.31-362817.4	37	7	63	4	26	5-6	5-10	0.02-0.04

Note. — [1]Number of sources in common between multiple Spitzer epochs. [2]Standard deviation of the mean of the central position of the combined Spitzer frames. [3]Limiting accuracy for any one source on single epoch, one axis. [4]Number of sources in common between Spitzer and HST frame, if available. [5]Standard deviation of the mean of the central positions between the Spitzer and HST frames. [6]Number of sources in common between Keck and Spitzer/HST frames. [7]Range in the standard deviation of the mean of the central positions between the Keck and Spitzer/HST frames. [8]Range in the precision of the determination of rotation angle between Keck and Spitzer/HST frames.

Table 6. Parallax and Proper Motion Solutions

WISE Designation	RA (J2000.0)	DEC (J2000.0)	$\mu_\alpha(''yr^{-1})^a$	$\mu_\delta(''yr^{-1})$	$\pi('')$	Dist (pc)	V_{tan}	$\chi^{2\ b}$	$\chi^{2\ c}$
J014656.66+423410.0	1h46m57.0940s±0.0112s	$42^o34'10.214''\pm0.''215$	-0.441±0.013	-0.026±0.016	0.094±0.014	10.6±1.5	22±3	23.0(27)	61.6(28)
J031358.93+780748.9	3h13m25.8000s±0.0097s	$78^o7'43.524''\pm0.''705$	0.080±0.012	0.072±0.057	0.153±0.015	6.5±0.6	3±1	21.4(17)	104.7(18)
J033515.01+431045.1	3h35m14.2520s±0.0096s	$43^o10'53.405''\pm0.''196$	0.826±0.011	-0.803±0.015	0.070±0.009	14.3±1.7	78±10	21.5(27)	71.4(28)
J041022.71+150248.4	4h10m22.0630s±0.0110s	$15^o3'11.053''\pm0.''158$	0.966±0.013	-2.218±0.013	0.160±0.009	6.2±0.4	72±4	23.7(33)	232.7(34)
J071322.55-291751.9	7h13m22.2510s±0.0166s	$-29^o17'47.558''\pm0.''277$	0.388±0.020	-0.419±0.022	0.106±0.013	9.4±1.2	26±3	17.4(19)	75.4(20)
J083641.10-185947.0	8h36m41.2030s±0.0061s	$-18^o59'45.080''\pm0.''086$	-0.038±0.007	-0.144±0.006	0.020±0.008	48.9±20.0	35±14	3.9(13)	5.6(14)
J131106.20+012254.3	13h11m6.0538s±0.0135s	$1^o23'2.850''\pm0.''2$	0.280±0.016	-0.838±0.016	0.062±0.012	16.1±3.0	68±13	13.0(17)	34.8(18)
J154151.65-225024.9	15h41m52.2500s±0.0100s	$-22^o50'24.540''\pm0.''162$	-0.857±0.012	-0.087±0.013	0.176±0.009	5.7±0.3	23±1	16.8(19)	354.0(20)
J154214.00+223005.2	15h42m14.7040s±0.0200s	$22^o30'9.098''\pm0.''33$	-0.960±0.024	-0.374±0.026	0.096±0.041	10.4±4.5	51±22	23.6(13)	32.9(14)
J173835.53+273259.0	17h38m35.2890s±0.0076s	$27^o33'2.091''\pm0.''128$	0.317±0.009	-0.321±0.011	0.128±0.010	7.8±0.6	17±1	19.4(27)	122.9(28)
J180435.37+311706.4	18h4m35.5700s±0.0082s	$31^o17'6.105''\pm0.''143$	-0.269±0.010	0.035±0.011	0.080±0.010	12.6±1.6	16±2	23.8(27)	69.7(28)
J182831.08+265037.7	18h28m30.2950s±0.0059s	$26^o50'36.030''\pm0.''075$	1.024±0.007	0.174±0.006	0.106±0.007	9.4±0.6	46±3	34.5(39)	234.6(40)
J205628.91+145953.2	20h56m28.3190s±0.0072s	$14^o59'47.804''\pm0.''097$	0.812±0.009	0.534±0.008	0.140±0.009	7.1±0.5	33±2	27.1(35)	201.7(36)
J220905.73+271143.9	22h9m4.7813s±0.0111s	$27^o11'58.336''\pm0.''185$	1.217±0.013	-1.372±0.015	0.147±0.011	6.8±0.5	59±4	15.1(19)	148.1(20)
J222055.31-362817.4	22h20m55.0650s±0.0122s	$-36^o28'16.312''\pm0.''227$	0.283±0.013	-0.097±0.017	0.136±0.017	7.4±0.9	10±1	16.8(17)	69.0(18)

Note. — [a]Proper motion in right ascension is given in units of $''yr^{-1}$ and includes the correction for $cos(\delta)$. [b] χ^2 value with degrees of freedom in parentheses. Fit includes parallax.[c] χ^2 value with degrees of freedom in parentheses. Fit does not include parallax.

Table 7. Kirkpatrick et al. Parallax Comparison

WISE Designation	Kirkpatrick Distance (pc)[1]	Keck Distance (pc)	Kirkpatrick/Keck Ratio
J014656.66+423410.0	6.3	10.6±1.5	0.6±0.1
J031325.96+780744.2	8.6	6.5±0.6	1.3±0.1
J033515.01+431045.1	14.0	14.3±1.7	1.0±0.1
J041022.71+150248.5[2]	6.1	6.2±0.4	1.0±0.1
J071322.55-291751.9	7.1	9.4±1.2	0.8±0.1
J083641.12-185947.2	22.2	48.9±20.0	0.5±0.2
J131106.24+012252.4	13.6	16.1±3.0	0.8±0.2
J154151.66-225025.2	4.2	5.7±0.3	0.7±0.0
J154214.00+223005.2	12.6	10.4±4.5	1.2±0.5
J173835.53+273258.9[2]	9.0	7.8±0.6	1.2±0.1
J180435.40+311706.1	9.2	12.6±1.6	0.7±0.1
J182831.08+265037.8[2]	8.2	9.4±0.6	0.9±0.1
J205628.90+145953.3	5.2	7.1±0.5	0.7±0.0
J222055.32-362817.5	8.1	7.4±0.9	1.1±0.1
Average[3]			0.9±0.2

Note. — [1]"Adopted" distance in Kirkpatrick et al. (2012); [2] Kirkpatrick et al (2012) distance was based on trig parallax (Marsh et al. 2013).[3]Average value of distance ratio for 12 sources with fractional uncertainties <20%.

Table 8. Dupuy & Kraus Parallax Comparison

WISE Designation	$\Delta\ Parallax/\sigma^1_{tot}$	$\Delta\ \mu RA/\sigma^1_{tot}$	$\Delta\ \mu Dec/\sigma^a_{tot}$	Dupuy Distance (pc)	This paper, (pc)
J041022.71+150248.5	1.6	-0.2	0.0	7.6±0.9	6.2±0.4
J154151.65-225025.2[2]	3.2	-0.7	-0.1	13.5±5.7	5.7±0.3
J173835.52+273258.9	1.3	-0.4	0.1	9.8±1.7	7.8±0.6
J180435.40+311706.1	1.3	1.0	0.0	16.7±3.1	12.6±1.6
J182831.08+265037.8	2.3	-0.3	0.0	14.3±2.9	9.4±0.6
J205628.90+145953.3	-0.1	-1.1	0.0	6.9±1.1	7.1±0.5

Note. — [a]Difference between values in this paper and Dupuy & Kraus (2013) relative to the combined uncertainties.[2]Obvious confusion in Spitzer data with neighboring star affects Spitzer-only parallax determination.

Table 9. BT-Settl Model Parameters[a]

WISE Designation	Spectral Type	Age (Gyr)	Mass (M_{Jup})	T_{eff} (K)	Radius (R_{Jup})	Log g (cm s^{-2})	χ^2	d.o.f
J014656.66+423410.0	Y0	3.4±2.5	14.4±5.5	451±23	0.97	4.61	9.1	2
J031358.93+780748.9	T8.5	8.8±0.4	26.2±1.7	651±46	0.88	4.95	17.4	2
J033515.01+431045.1	T9	8.0±0.4	21.8±1.1	465±23	0.90	4.84	54.2	3
J041022.71+150248.4	Y0	8.0±0.4	18.2±0.9	409±20	0.92	4.75	25.4	3
J071322.55-291751.9	Y0	7.5±1.1	19.5±1.8	422±21	0.92	4.78	18.1	2
J083641.10-185947.0	T8p	4.2±3.1	26.2±9.1	662±52	0.90	4.93	2.9	2
J131106.20+012254.3	T9	7.6±2.6	27.0±3.5	641±53	0.88	4.96	7.2	2
J154151.65-225024.9[b]	Y0.5	5.0±2.0	12.0±3.0	350±25	1.0	4.50	410	3
J154214.00+223005.2	T9.5	8.5±0.4	19.4±1.0	477±24	0.91	4.78	11.2	4
J173835.53+273259.0	Y0	8.2±0.4	18.6±0.9	409±20	0.92	4.76	47.1	3
J180435.37+311706.4	T9.5:	5.2±1.1	27.9±2.1	583±29	0.89	4.97	2.4	2
J182831.08+265037.7[b]	≥Y2	5.0±2.0	12.0±3.0	350±25	1.0	4.50	3,700	4
J205628.91+145953.2	Y0	8.0±2.0	17.0±0.9	407±20	0.93	4.71	112.5	3
J220905.73+271143.9[b]	Y0:	5.0±2.0	12.0±0.6	350±25	1.0	4.10	1,000	2
J222055.31-362817.4	Y0	7.6±0.4	14.1±0.8	404±20	0.95	4.61	5.5	3
Average		6.6	19.4	473	0.93	4.72	387.5	
Dispersion		1.9	5.7	114	0.04	0.23	993.6	
Median		7.6	19.0	437	0.92	4.76	21.8	

Note. — [a]Fits of photometry to BT-Settl model (Allard et al. 2003, 2010). Uncertainties in the model parameters are the larger of the dispersion in Monte Carlo calculations or 10%. [b]As discussed in the text, these models fits were derived using a coarse low temperature grid (≤400 K) with uncertainties based on grid spacing. These model values should be regarded as quite uncertain.

Table 10. Morley[a] Model Parameters

WISE Designation	Spectral Type	Age[b] (Gyr)	Mass (M_{Jup})	T_{eff} (K)	Rad (R_{Jup})	Log g cm s^{-2}	Sed	χ^2	d.o.f	ΔT[c] (K)	Mass Ratio[d]	ΔAge Gyr[e]
J014656.66+423410.0	Y0	6	31.9±0.1	570±13	0.89	5.00±0.05	5	46.5	2	119	2.0	2.7
J031358.93+780748.9	T8.5	4	32.4±1.1	662±7	0.90	5.00±0.05	3	28.7	2	11	2.0	-5.0
J033515.01+431045.1	T9	3	25.2±3.9	605±10	0.95	4.85±0.22	2	24.6	3	140	3.0	-5.2
J041022.71+150248.4	Y0	6	25.3±1.8	491±5	0.92	4.87±0.10	5	137.6	3	82	3.0	-2.2
J071322.55-291751.9	Y0	8	31.5±0.1	513±7	0.88	5.00±0.00	4	28.0	2	90	2.0	0.9
J083641.10-185947.0	T8p	3	33.1±1.0	765±18	0.91	4.99±0.04	2	15.8	2	103	2.0	-1.7
J131106.20+012254.3	T9	3	31.0±3.4	672±12	0.91	4.97±0.16	5	9.2	2	31	2.0	-4.3
J154151.65-225024.9[b]	Y0.5	14	30.8±0.0	441±4	0.87	5.00±0.05	2	193.2	3	91	3.0	8.9
J154214.00+223005.2	T9.5	6	31.8±0.1	563±5	0.89	5.00±0.00	4	36.6	4	86	4.0	-2.2
J173835.53+273259.0	Y0	8	31.3±0.6	514±6	0.89	5.00±0.03	5	120.2	3	105	3.0	0.1
J180435.37+311706.4	T9.5:	3	32.3±1.4	706±7	0.91	4.99±0.06	3	47.3	2	122	2.0	-2.1
J182831.08+265037.7[b]	≥Y2	15	22.0±1.0	400±40	0.74	5.00±0.05	2	1,468.9	4	50	4.0	10.0
J205628.91+145953.2	Y0	10	31.2±0.1	488±4	0.88	5.00±0.01	5	216.0	3	81	3.0	1.8
J220905.73+271143.9[b]	Y0:	15	22.0±1.0	400±40	0.74	5.00±0.05	2	387.9	2	50	2.0	10.0
J222055.31-362817.4	Y0	8	31.3±1.4	525±6	0.89	4.99±0.06	2	57.4	3	127	3.0	0.3
Average		7.4	29.4	556	0.88	4.98		197		83	1.6	0.8
Dispersion		4.5	4.0	114	0.06	4.00		381		88	1.6	5.3
Median		6.2	31.3	538	0.89	5.00		47		36	0.4	-0.8

Note. — [a] Fits of photometry to Morley et al. models as described in Morley et al. (2012); Leggett et al. (2012); Saumon & Marley (2008). [b] Ages interpolated from Figure 4 in Saumon & Marley (2008) for cloudy models with *sed*=2; [c] In the sense T_{Morley}-$T_{BTSettl}$; [d] In the sense $M_{Morley}/M_{BTSettl}$; [e] In the sense Age_{Morley}-$Age_{BTSettl}$

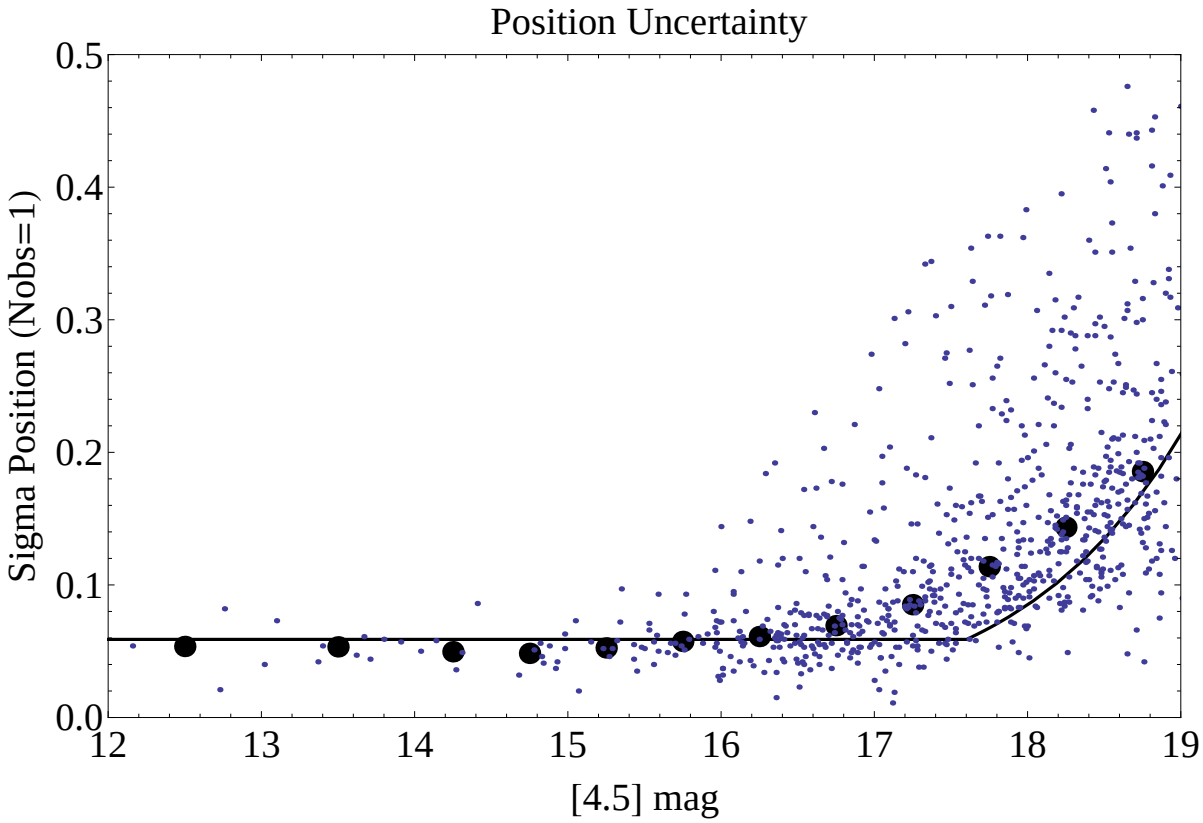


Fig. 1.— The dispersion in Spitzer positions from one epoch to the next is shown as a function of [4.6] Spitzer magnitude. Individual reference sources (small circles) were used to register the Spitzer frames and were drawn from a region within 60″ - 90″ of each brown dwarf target. The single axis uncertainties have been normalized to a single epoch according to $N_{obs}^{1/2}$ and are thus representative of the uncertainties for our single epoch brown dwarf measurements. The large filled circles represent the median uncertainty in 0.5 mag wide bins (1.0 mag bins for the 2 brightest bins). The solid line shows a model fitted to these values with a constant uncertainty of $\sigma_0 = 58 \pm 8$ mas for sources brighter than [4.6]<17.6±0.2 mag and an uncertainty increasing as SNR^{-1} for fainter objects. Outliers in the distribution are typically due to confused or extended sources. Our brown dwarf targets are located in bright source portion of the positional uncertainty distribution.

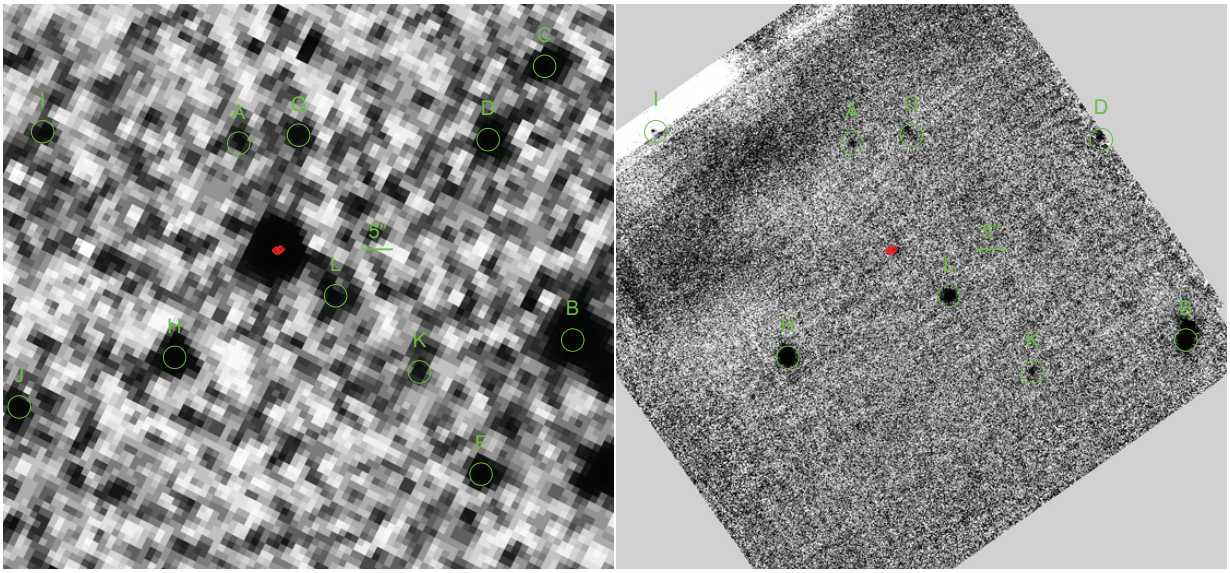


Fig. 2.— Spitzer (left) and Keck (right) images at 4.6 μm and 1.65 μm, respectively, of WISE 0146+4234 with the reference stars used for the co-registration of the fields circled in green. The positions of the brown dwarf are marked in red. A scale bar denotes 5″.

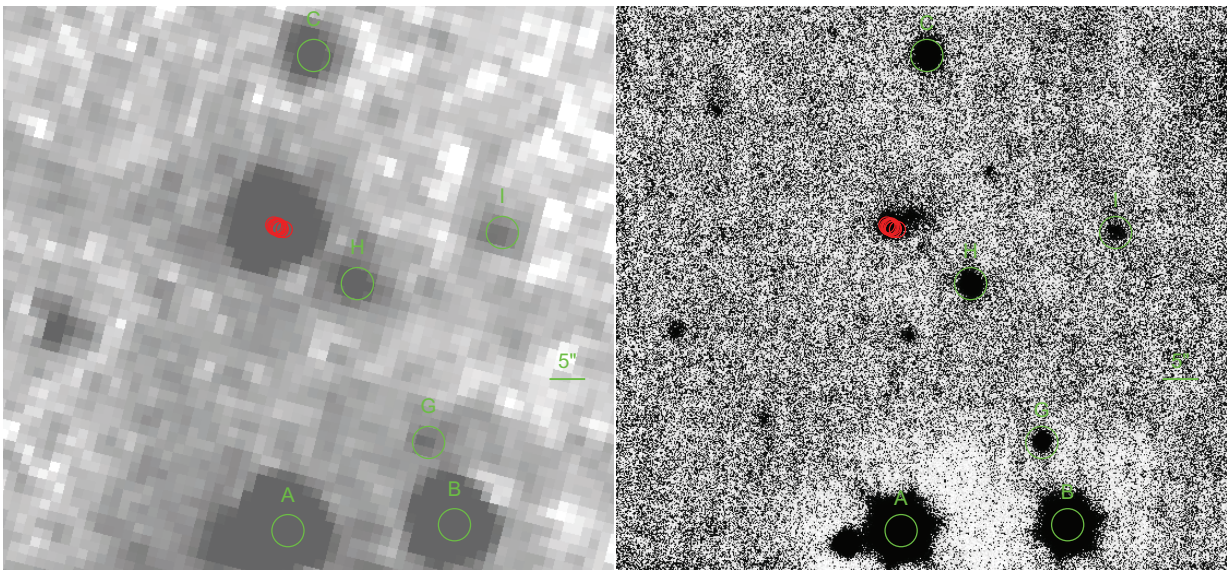


Fig. 3.— Spitzer (left) and Keck (right) images at 4.6 μm and 1.65 μm, respectively, of WISE 0313+7807 with the reference stars used for the co-registration of the fields circled in green. The positions of the brown dwarf are marked in red. A scale bar denotes 5″. A faint galaxy near the source does not affect the astrometry or the mid-IR photometry.

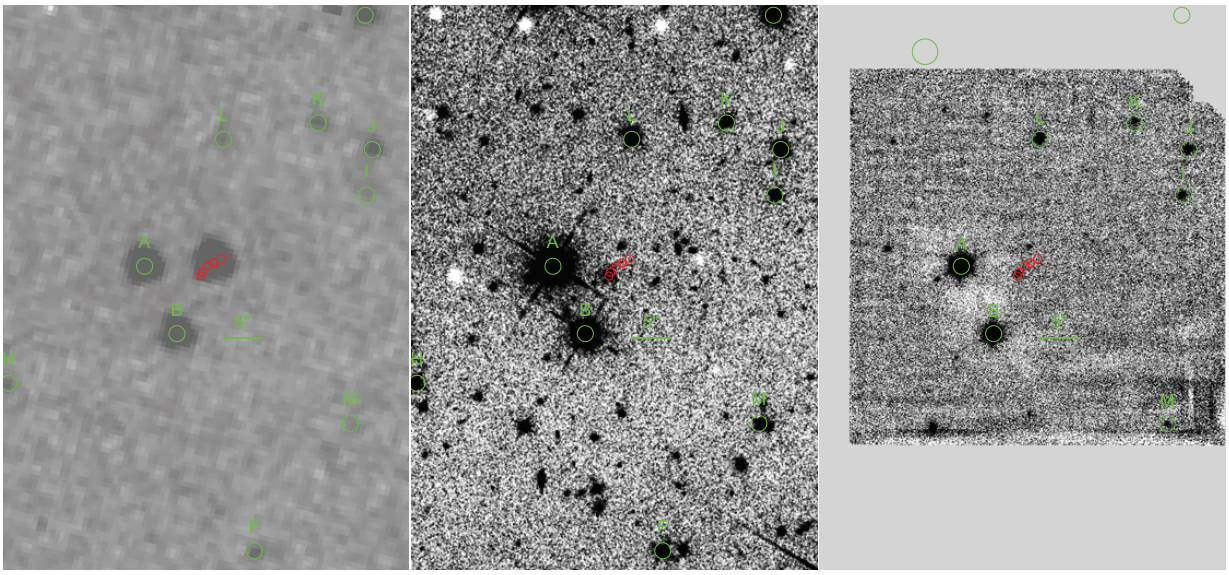


Fig. 4.— Spitzer Space Telescope (left), Hubble Space Telescope (HST,center) and Keck (right) images at 4.6 μm, F125W and H, respectively, of WISE 0335+4310 with the reference stars used for the co-registration of the fields circled in green. The positions of the brown dwarf are marked in red. A scale bar denotes 5″.

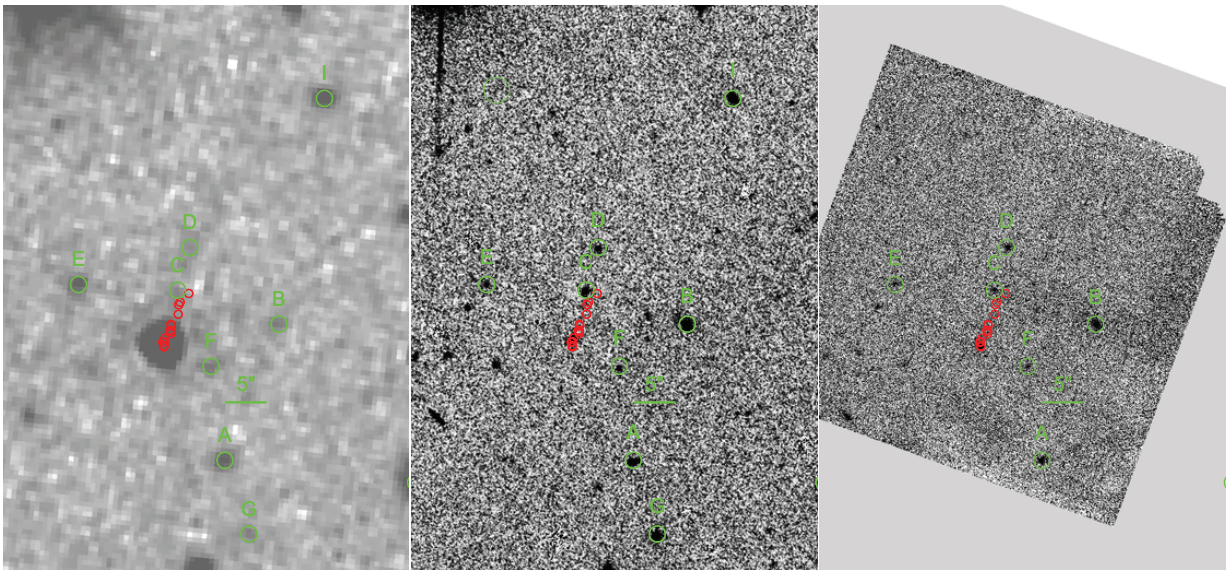


Fig. 5.— Spitzer Space Telescope (left), Hubble Space Telescope (HST,center) and Keck (right) images at 4.6 μm, F125W and H, respectively, of WISE 0410+1502 with the reference stars used for the co-registration of the fields circled in green. The positions of the brown dwarf are marked in red. A scale bar denotes 5″.

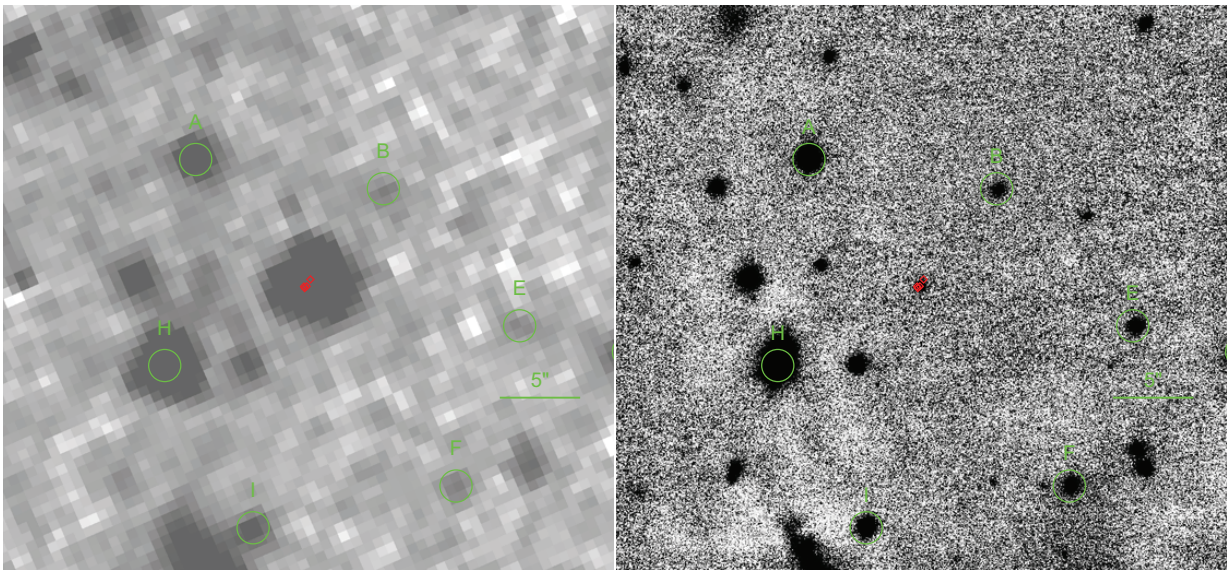


Fig. 6.— Spitzer (left) and Keck (right) images at 4.6 μm and 1.65 μm, respectively, of WISE 0713-2917 with the reference stars used for the co-registration of the fields circled in green. The positions of the brown dwarf are marked in red. North is up and East is to the left. A scale bar denotes 5″.

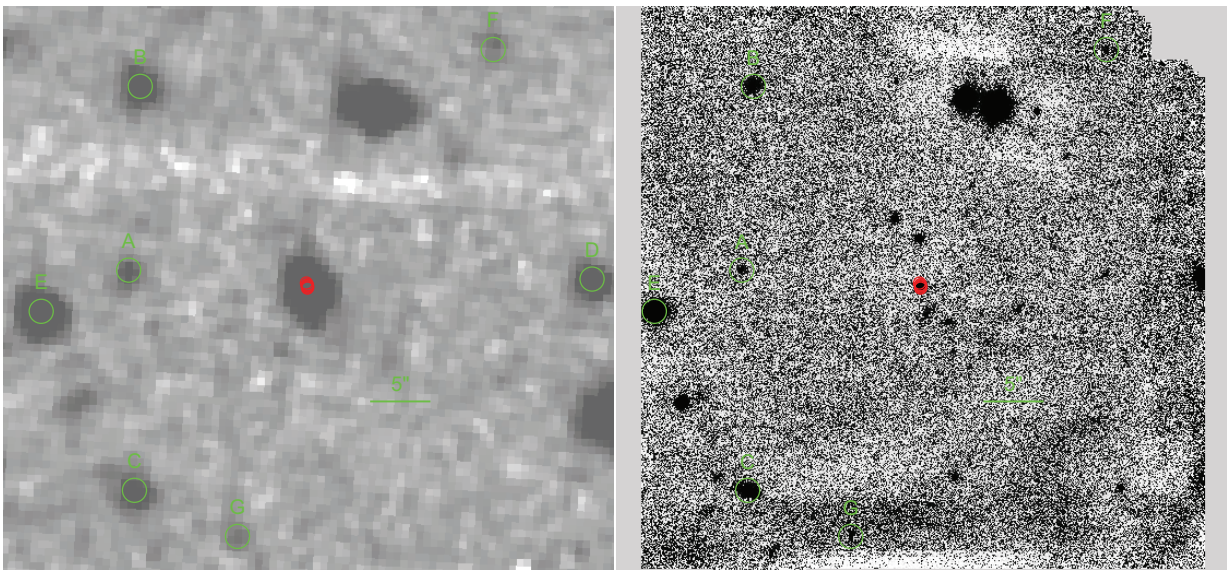


Fig. 7.— Spitzer (left) and Keck (right) images at 4.6 μm and 1.65 μm, respectively, of WISE 0836-1859 with the reference stars used for the co-registration of the fields circled in green. The positions of the brown dwarf are marked in red. North is up and East is to the left. A scale bar denotes 5″.

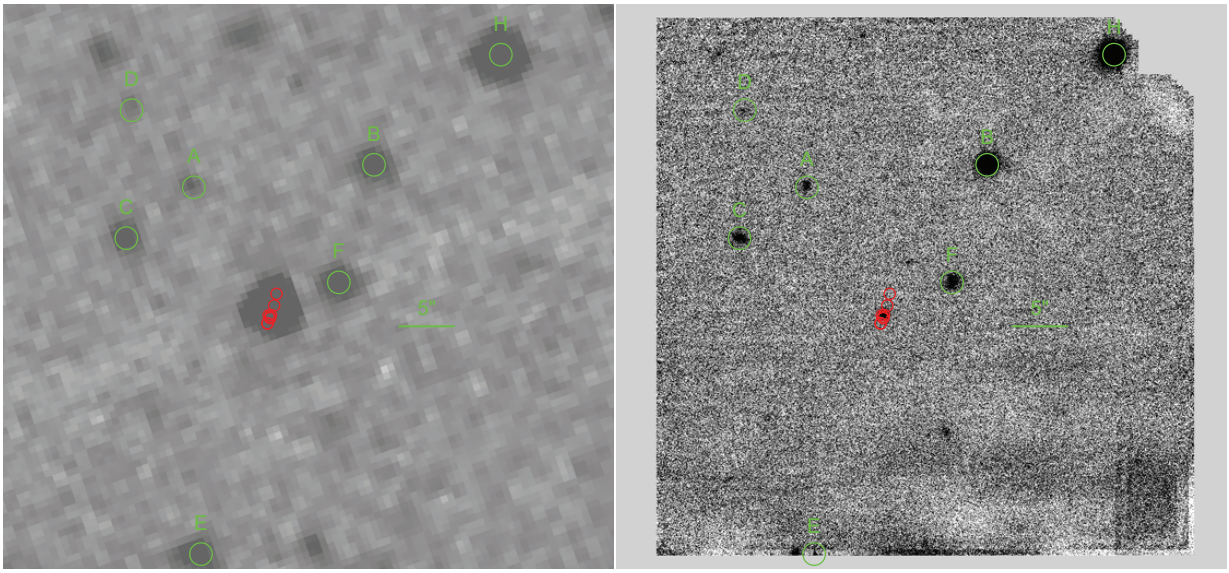


Fig. 8.— Spitzer (left) and Keck (right) images at 4.6 μm and 1.65 μm, respectively, of WISE 1311+0122 with the reference stars used for the co-registration of the fields circled in green. The positions of the brown dwarf are marked in red. North is up and East is to the left. A scale bar denotes 5″.

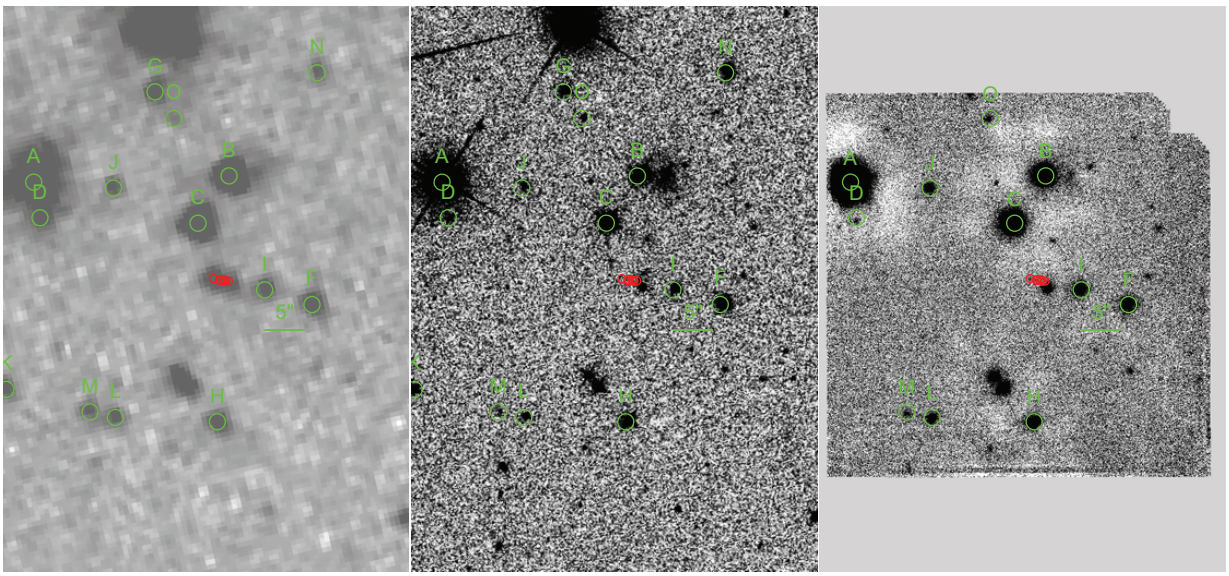


Fig. 9.— Spitzer Space Telescope (left), Hubble Space Telescope (HST,center) and Keck (right) images at 4.6 μm, F125W and H, respectively, of WISE1541-2250 with the reference stars used for the co-registration of the fields circled in green. The positions of the brown dwarf are marked in red. North is up and East is to the left. A scale bar denotes 5″. Confusion with the star close to the brown dwarf is a problem for later Spitzer epochs and accordingly were not used in the astrometric solution.

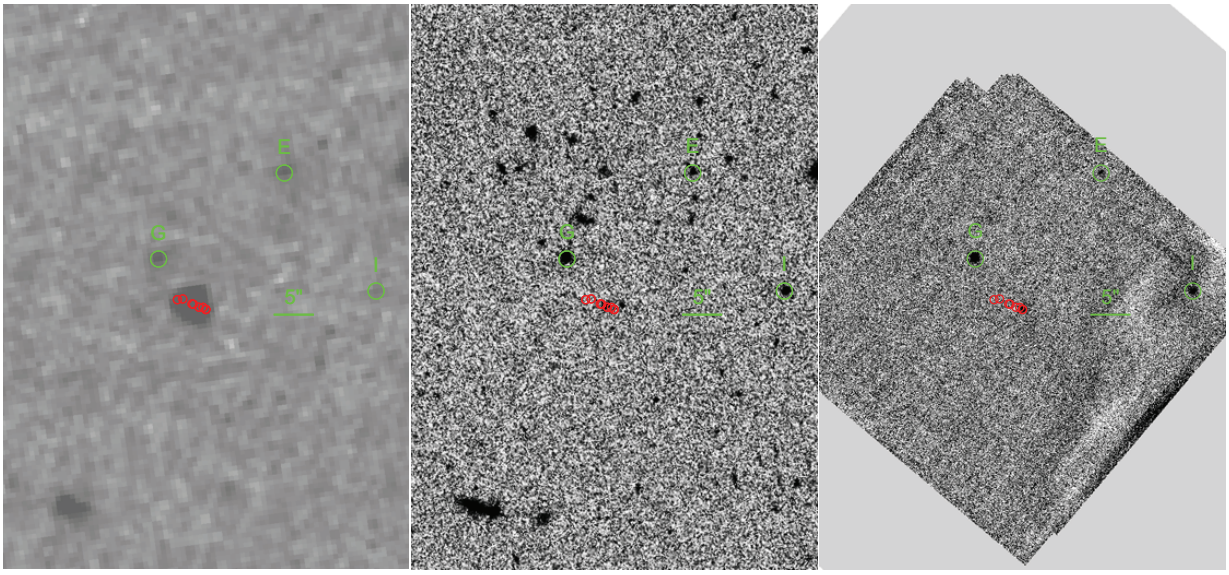


Fig. 10.— Spitzer Space Telescope (left), Hubble Space Telescope (HST,center) and Keck (right) images at 4.6 μm, F125W and H, respectively, of WISE 1542+2230 with the reference stars used for the co-registration of the fields circled in green. The positions of the brown dwarf are marked in red. North is up and East is to the left. A scale bar denotes 5″.

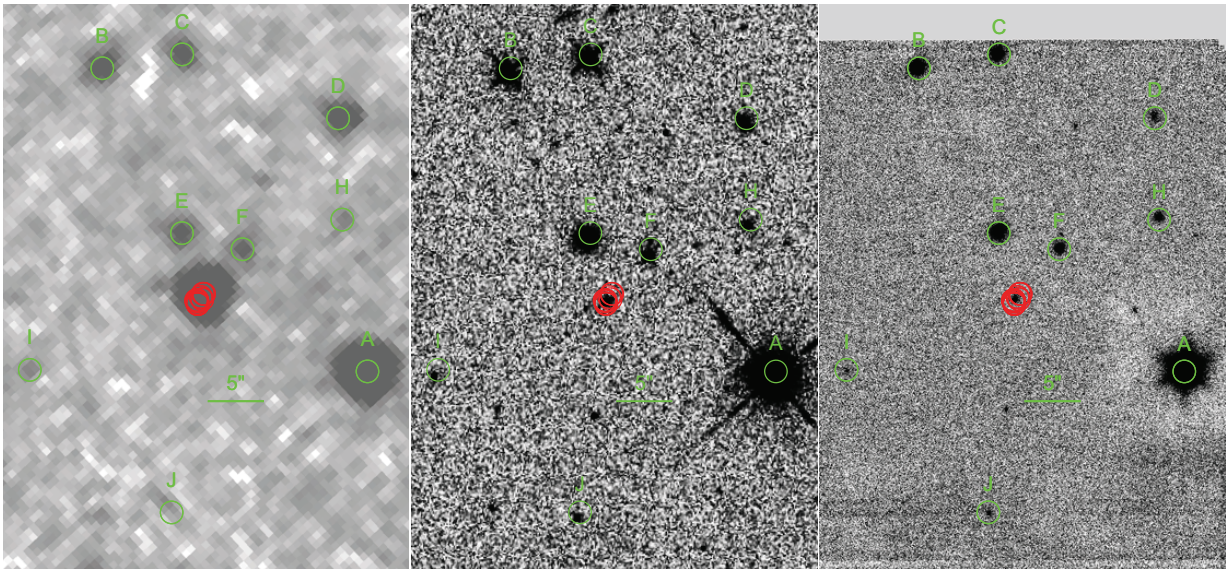


Fig. 11.— Spitzer Space Telescope (left), Hubble Space Telescope (HST,center) and Keck (right) images at 4.6 μm, F125W and H, respectively, of WISE 1738+2732 with the reference stars used for the co-registration of the fields circled in green. The positions of the brown dwarf are marked in red. North is up and East is to the left. A scale bar denotes 5″.

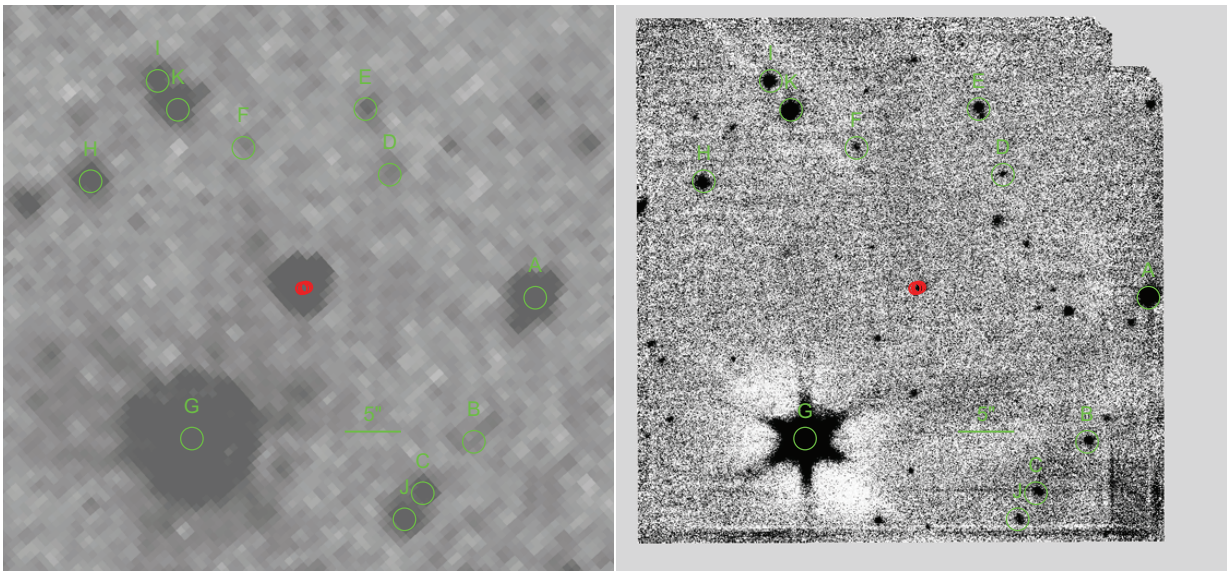


Fig. 12.— Spitzer (left) and Keck (right) images at 4.6 μm and 1.65 μm, respectively, of WISE1804+3117 with the reference stars used for the co-registration of the fields circled in green. The positions of the brown dwarf are marked in red. North is up and East is to the left. A scale bar denotes 5″.

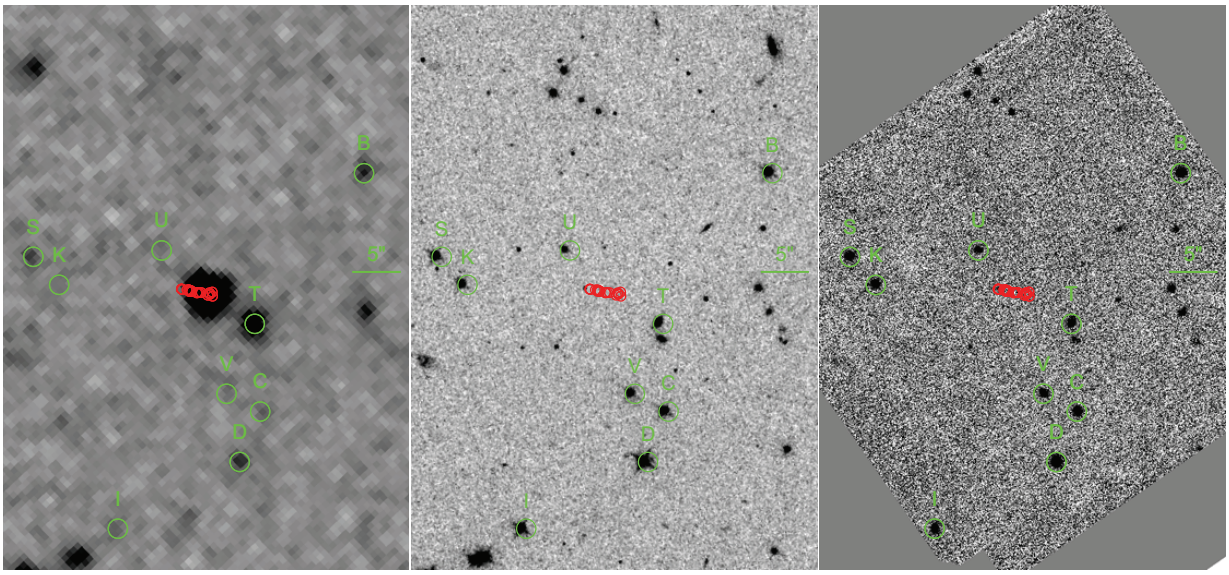


Fig. 13.— Spitzer Space Telescope (left), Hubble Space Telescope (HST,center) and Keck (right) images at 4.6 μm, F125W and H, respectively, of WISE 1828+2650 with the reference stars used for the co-registration of the fields circled in green. The positions of the brown dwarf are marked in red. North is up and East is to the left. A scale bar denotes 5″.

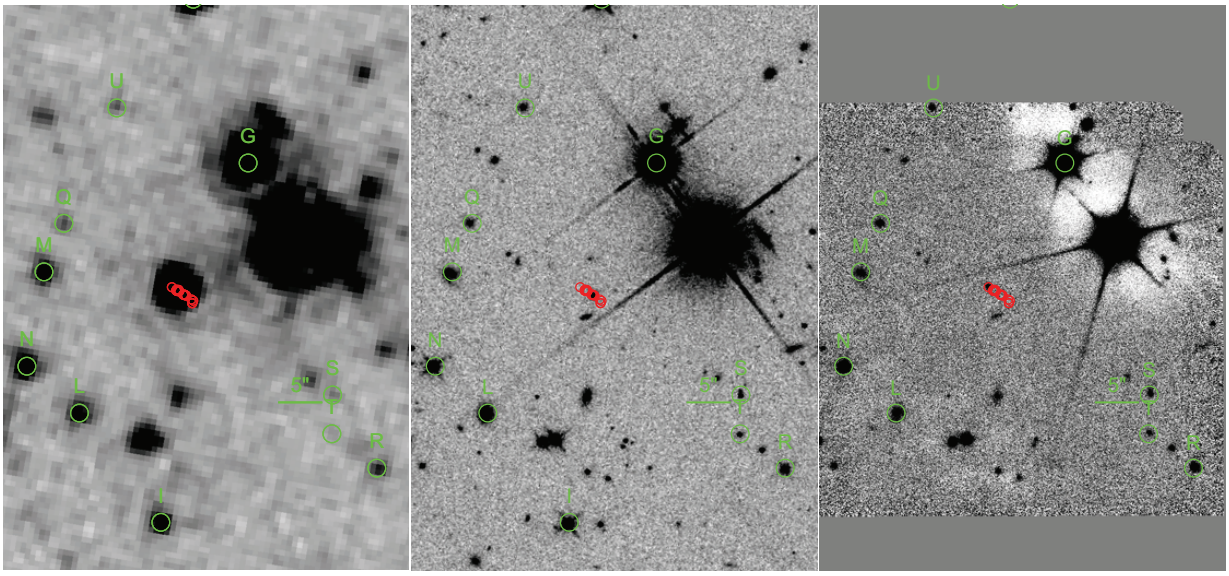


Fig. 14.— Spitzer Space Telescope (left), Hubble Space Telescope (HST,center) and Keck (right) images at 4.6 μm, F125W and H, respectively, of WISE2056+1459 with the reference stars used for the co-registration of the fields circled in green. The positions of the brown dwarf are marked in red. North is up and East is to the left. A scale bar denotes 5″.

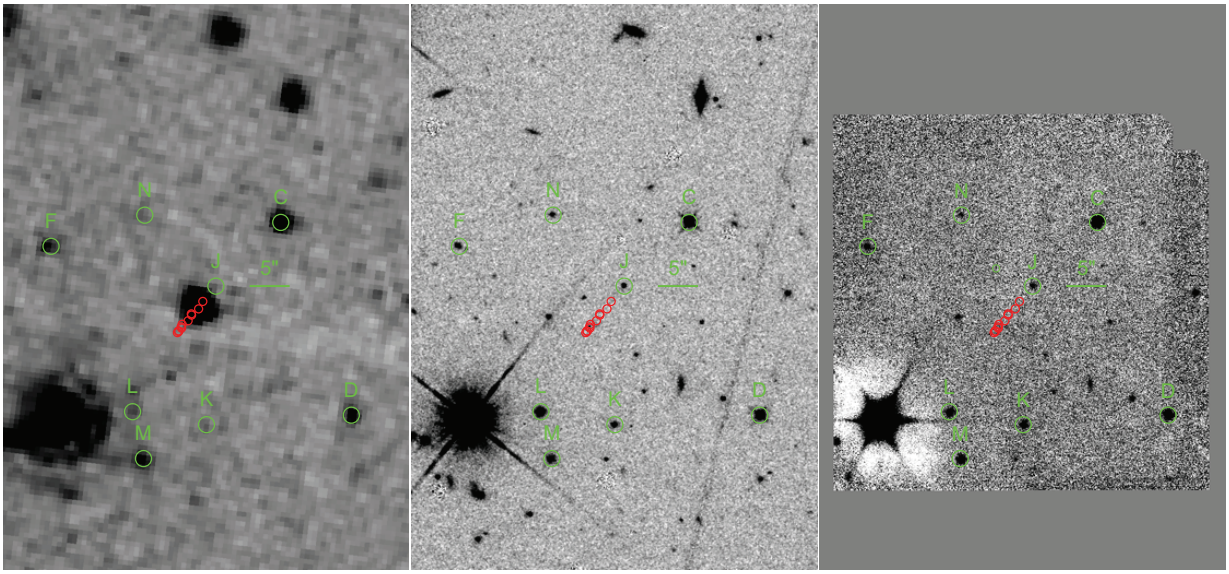


Fig. 15.— Spitzer Space Telescope (left), Hubble Space Telescope (HST,center) and Keck (right) images at 4.6 μm, F125W and H, respectively, of WISE 2209+2711 with the reference stars used for the co-registration of the fields circled in green. The position of the brown dwarf is marked in red. North is up and East is to the left. A scale bar denotes 5″.

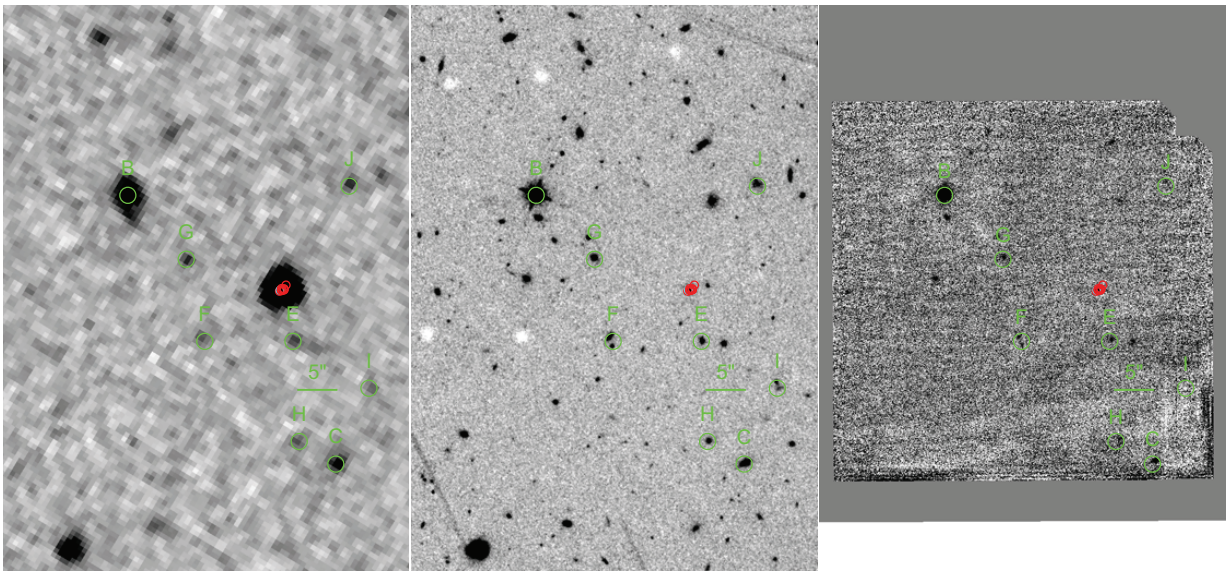


Fig. 16.— Spitzer Space Telescope (left), Hubble Space Telescope (HST,center) and Keck (right) images at 4.6 μm, F125W and H, respectively, of WISE 2220-3628 with the reference stars used for the co-registration of the fields circled in green. The position of the brown dwarf is marked in red. North is up and East is to the left. A scale bar denotes 5″.

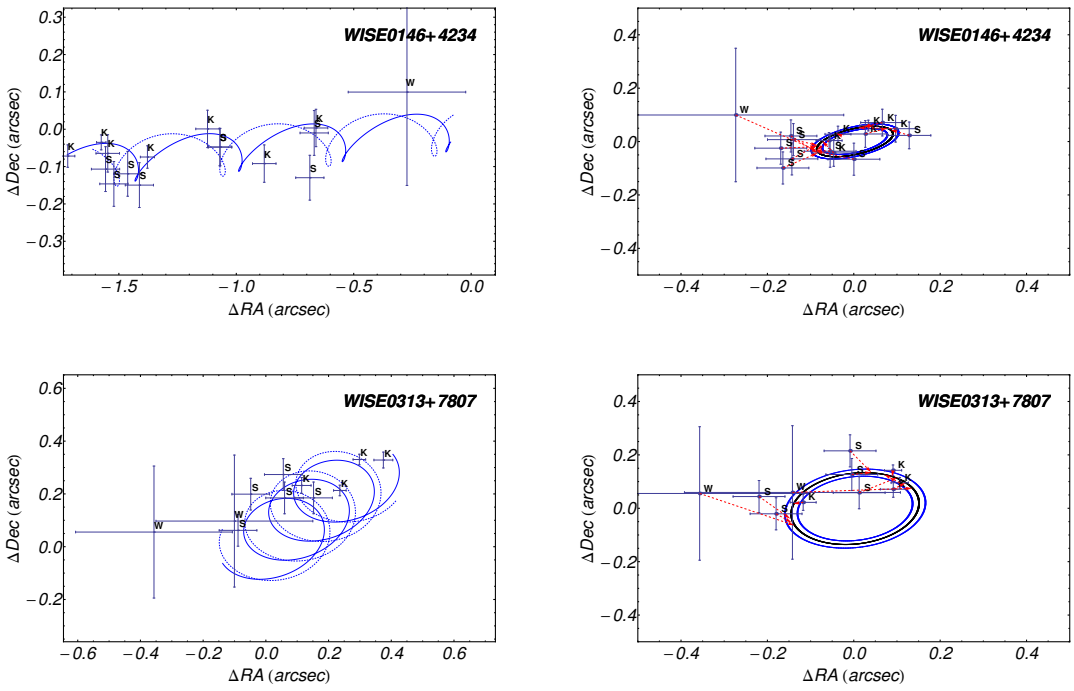


Fig. 17.— The parallactic solutions for two brown dwarfs, WISE0146+4234 (top) and WISE0313+7807 (bottom). In both figures, the left hand panel shows the total motion including both proper motion and parallax as seen from earth-centered observatories (solid line; WISE (W), Keck (K), or Hubble (H)) and the earth-trailing Spitzer (S) telescope (dotted line). The right-hand panel shows the derived parallactic ellipse with observations from the various facilities denoted with appropriate letter (K—Keck, S—Spitzer, W—WISE, H—Hubble. Arrows connect the data points to the points on ellipse appropriate to the observing epochs. Ellipses corresponding to $\pi \pm 1\sigma$ are also shown. Motion in right ascension is given in units of $''yr^{-1}$ and includes the correction for $cos(\delta)$.

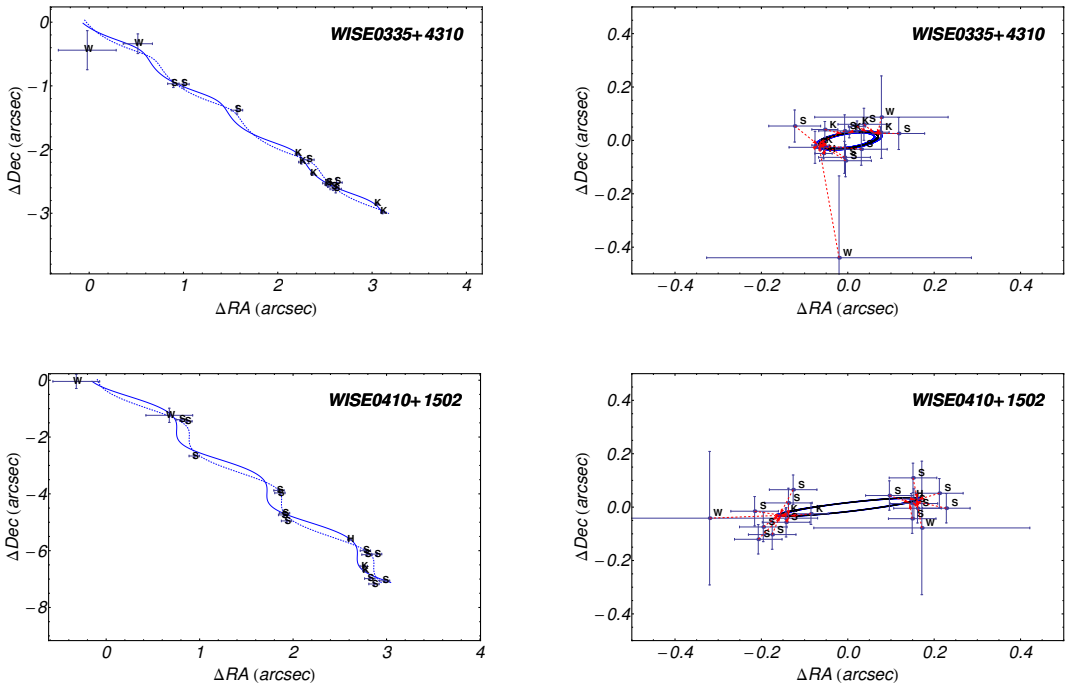


Fig. 18.— As described in Figure 17, the figure shows the parallactic solutions for two brown dwarfs, WISE0335+4310 (top) and WISE0410+1502 (bottom).

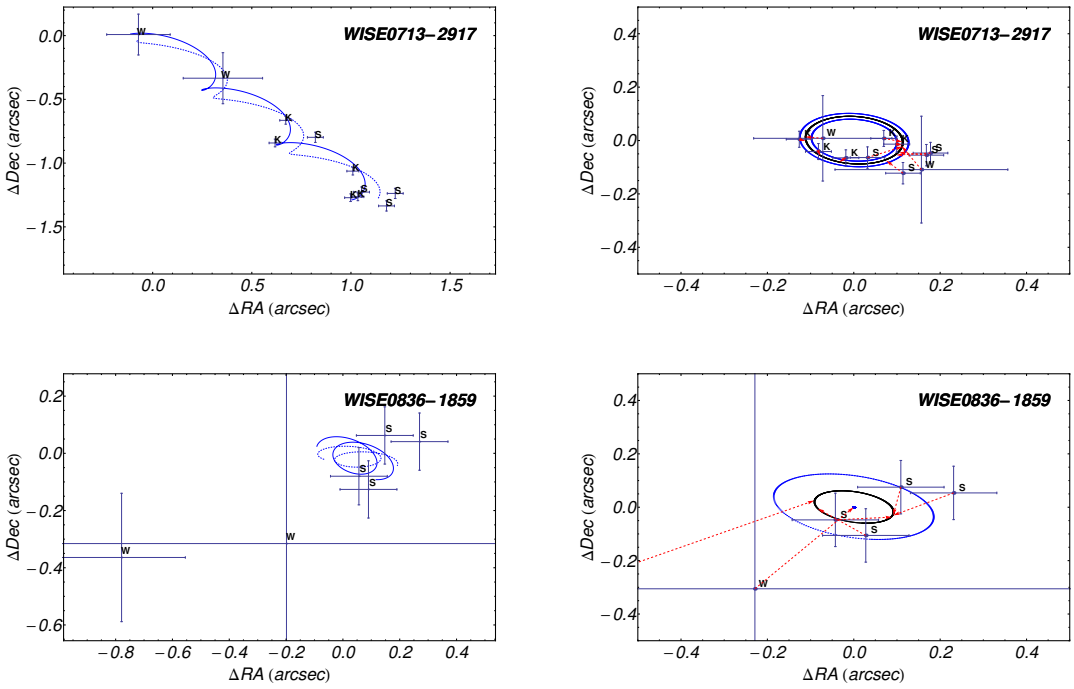


Fig. 19.— As described in Figure 17, the figure shows the parallactic solutions for two brown dwarfs, WISE0713-2917 (top) and WISE0836-1859 (bottom). The solution for WISE0836-1859 has relatively few data points and is poorly constrained

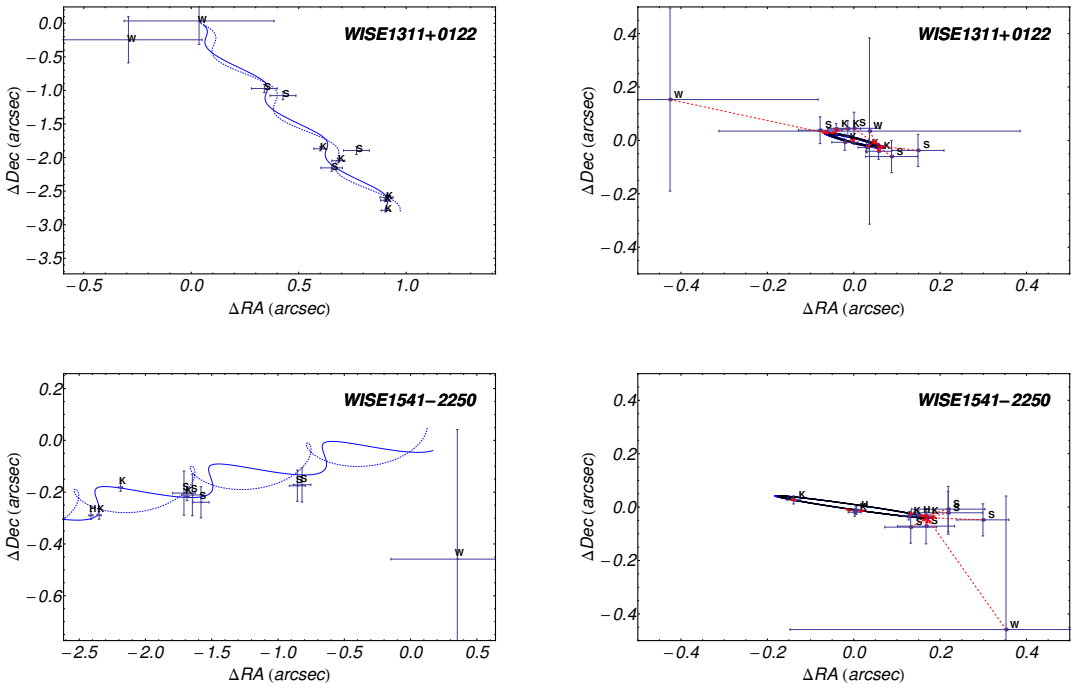


Fig. 20.— As described in Figure 17, the figure shows the parallactic solutions for two brown dwarfs, WISE1311+0122 (top) and WISE1541-2250 (bottom).

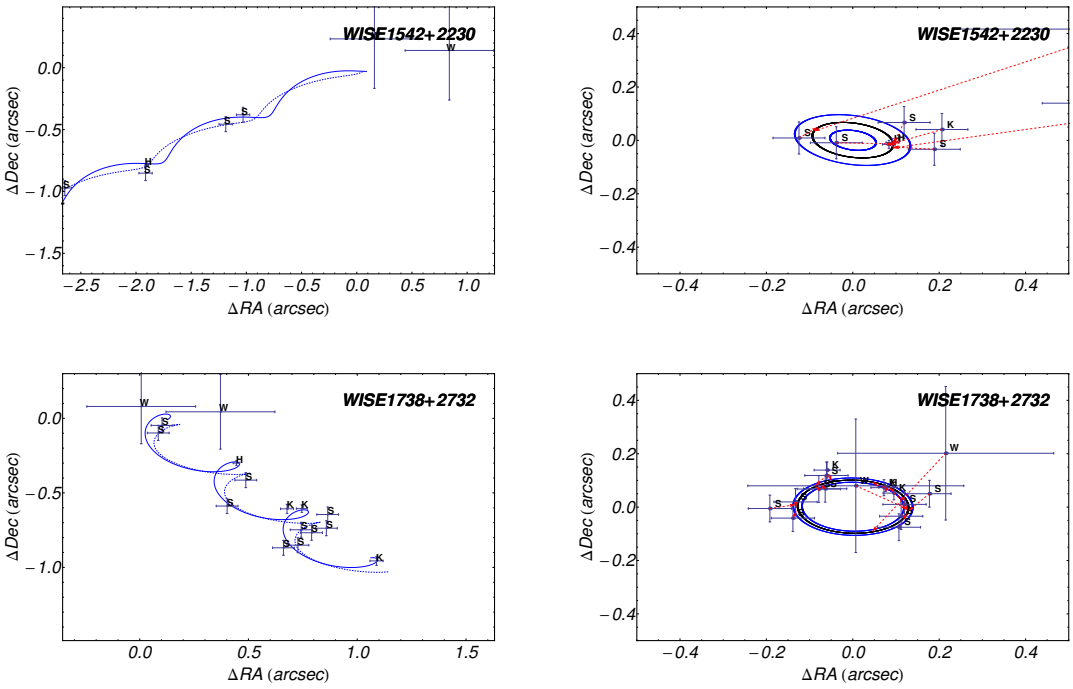


Fig. 21.— As described in Figure 17, the figure shows the parallactic solutions for two brown dwarfs, WISE1542+2230 (top) and WISE1738+2732 (bottom).

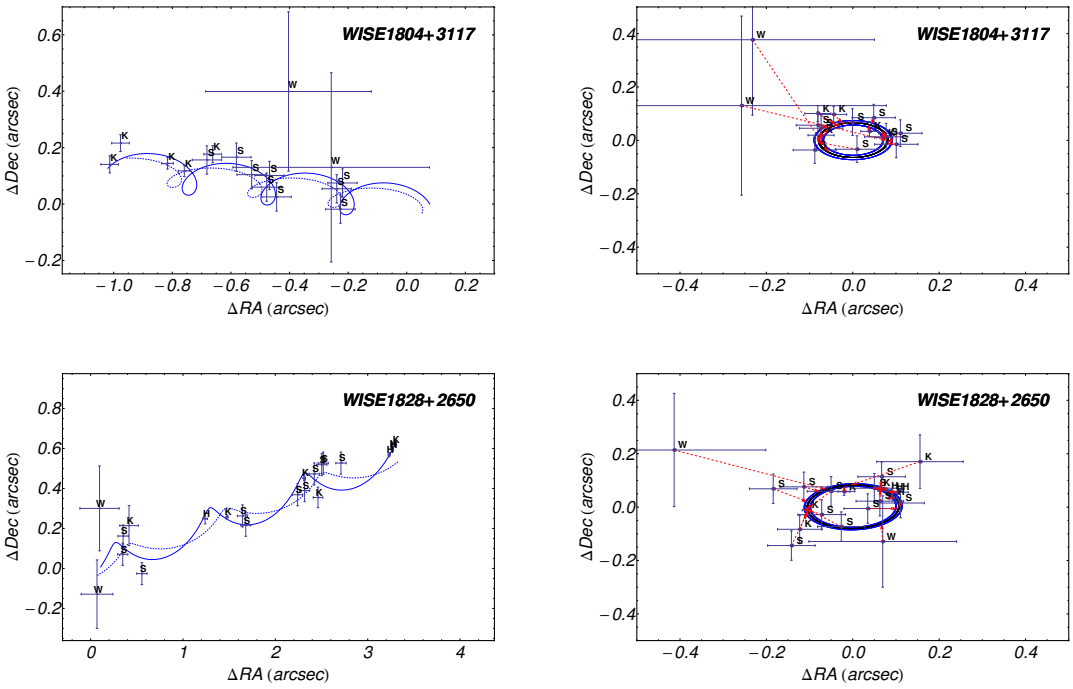


Fig. 22.— As described in Figure 17, the figure shows the parallactic solutions for two brown dwarfs, WISE1804+3117 (top) and WISE1828+2650 (bottom).

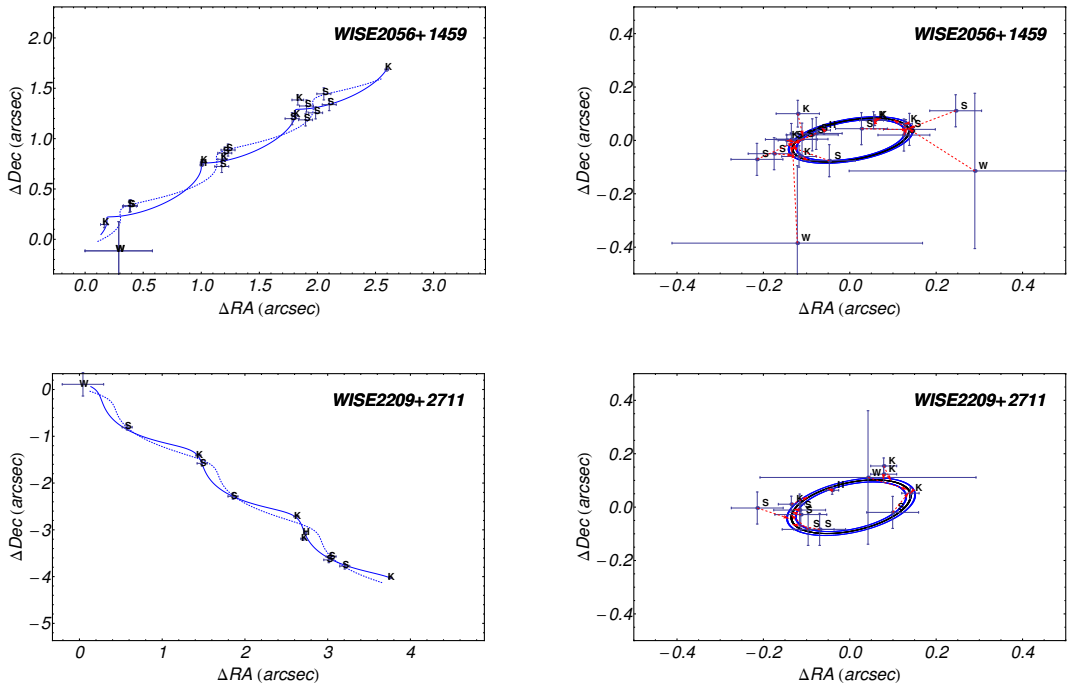


Fig. 23.— As described in Figure 17, the figure shows the parallactic solutions for two brown dwarfs, WISE2056+1459 (top) and WISE2209+2711 (bottom).

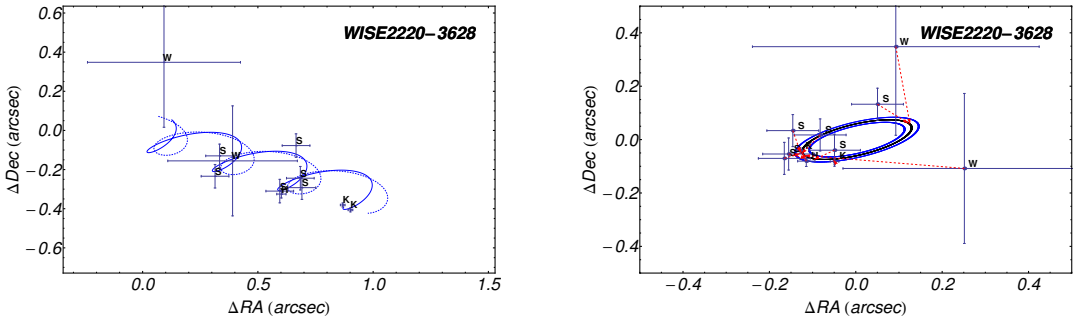


Fig. 24.— As described in Figure 17, the figure shows the parallactic solutions for the brown dwarf WISE2220-3628.

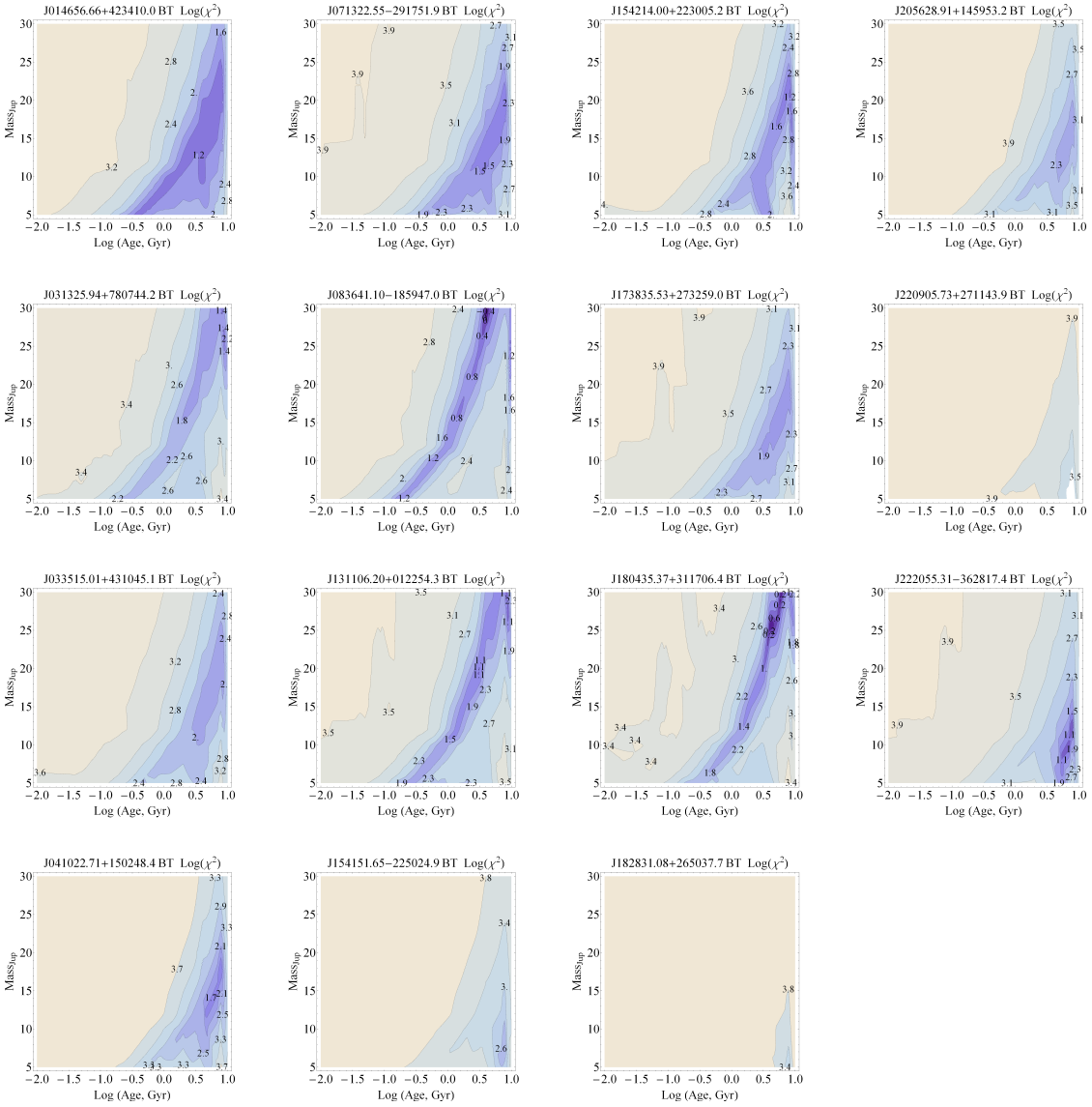


Fig. 25.— A sequence of fits of BTSettl models (Allard et al. 2003, 2010) to the absolute 4.5 μm brightness and to other mag_i-[4.5] colors for four of the late T and Y dwarfs in our sample. The plots show contours of the logarithm of the χ^2 parameter defined in Equation (3). The high values of χ^2 indicate that the BTSettl models are relatively poor fits to the spectral energy distributions of the very cold sources.

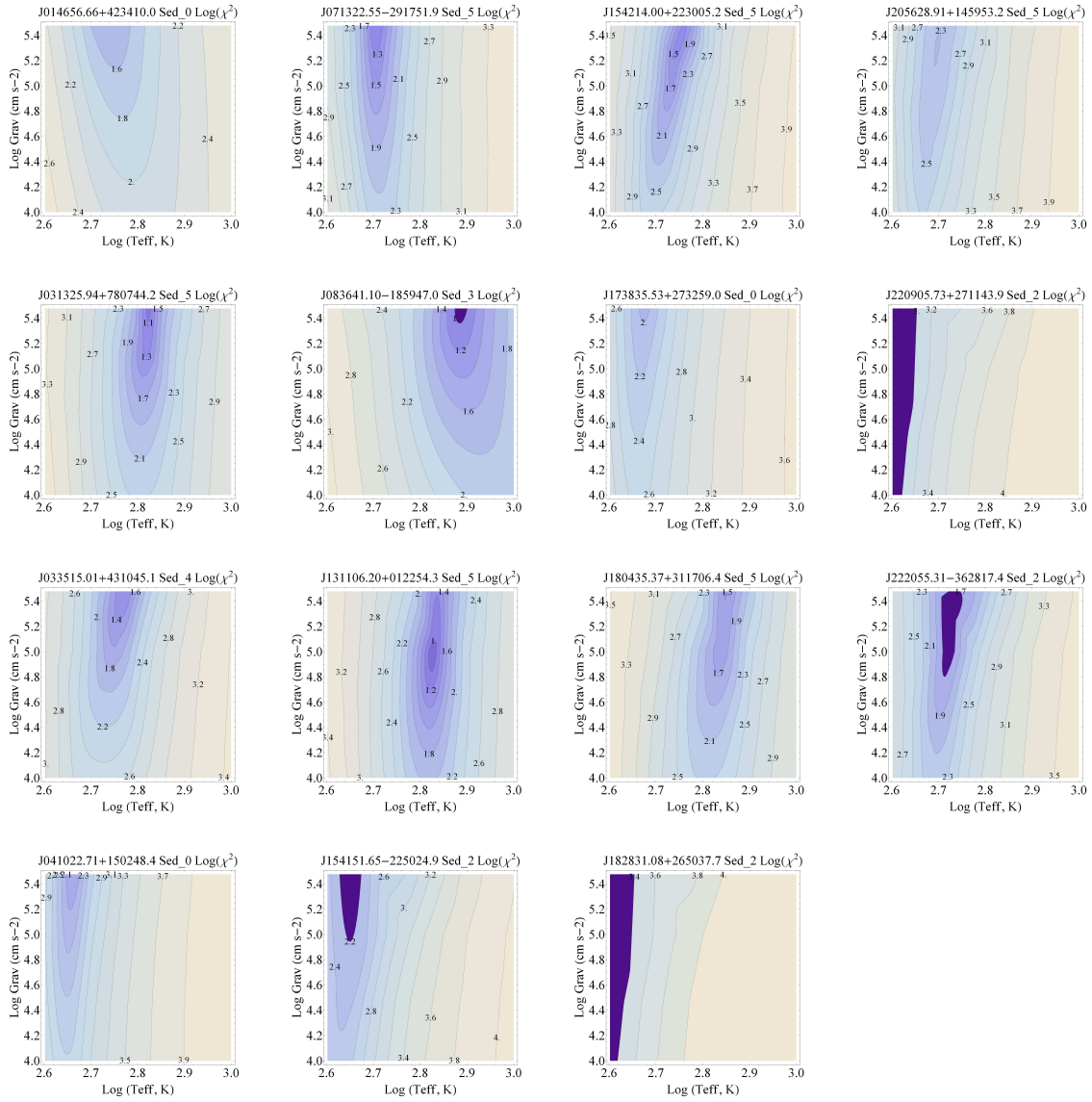


Fig. 26.— A sequence of fits of models (Morley et al. 2012)to the absolute 4.5 μm brightness and to other mag_i-[4.5] colors for four of the late T and Y dwarfs in our sample. The plots show contours of the logarithm of the χ^2 parameter defined in Equation (3). In each case the model shown represents a slice through the 3-D parameter space for the value of the sedimentation parameter, f_{sed}, that best fits the data. The f_{sed} value is given at the top of each plot.

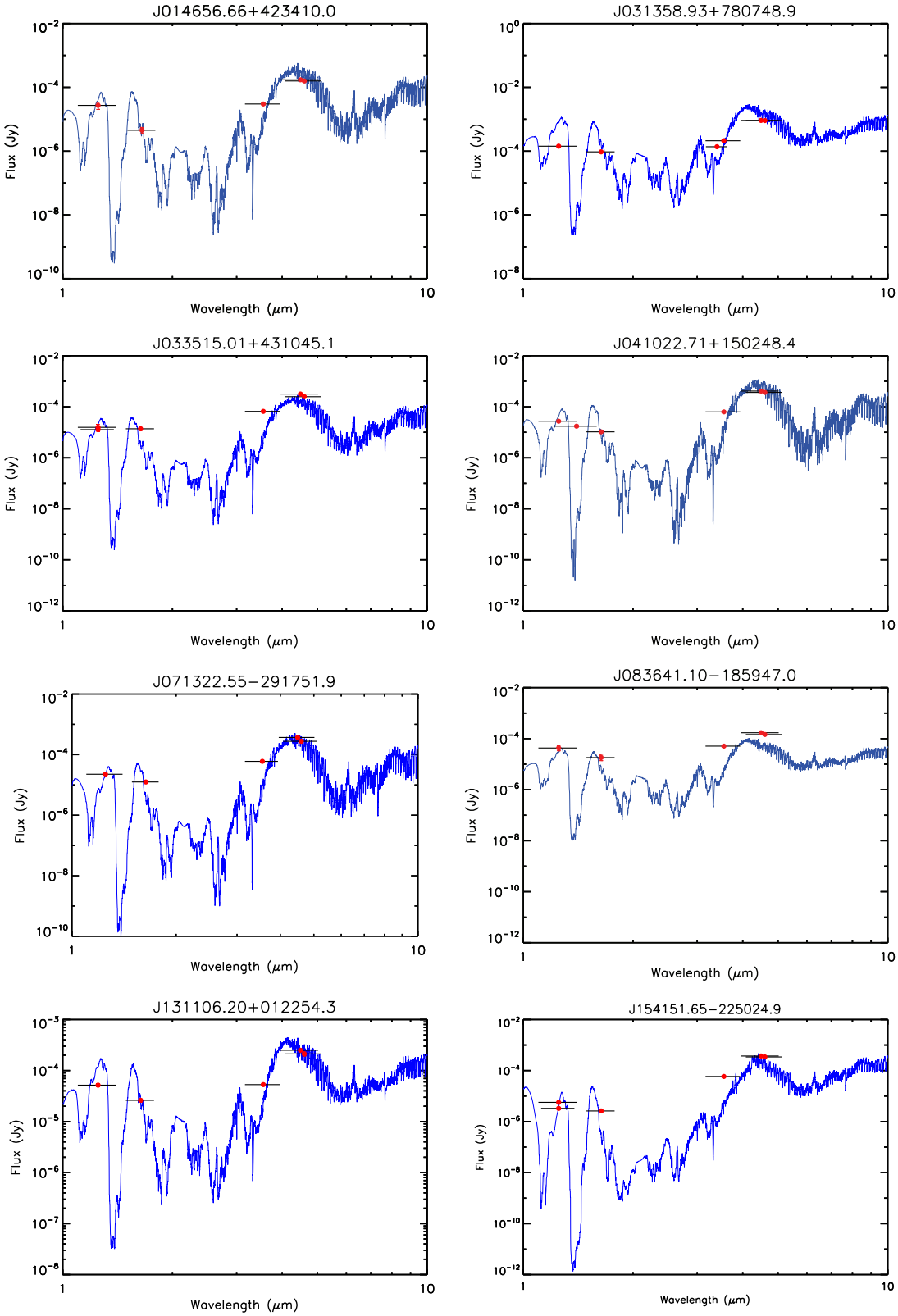


Fig. 27.— a-h). The result of fitting the photometric colors and absolute absolute 4.5 μm brightness to the BT-Settl models as described in the text.

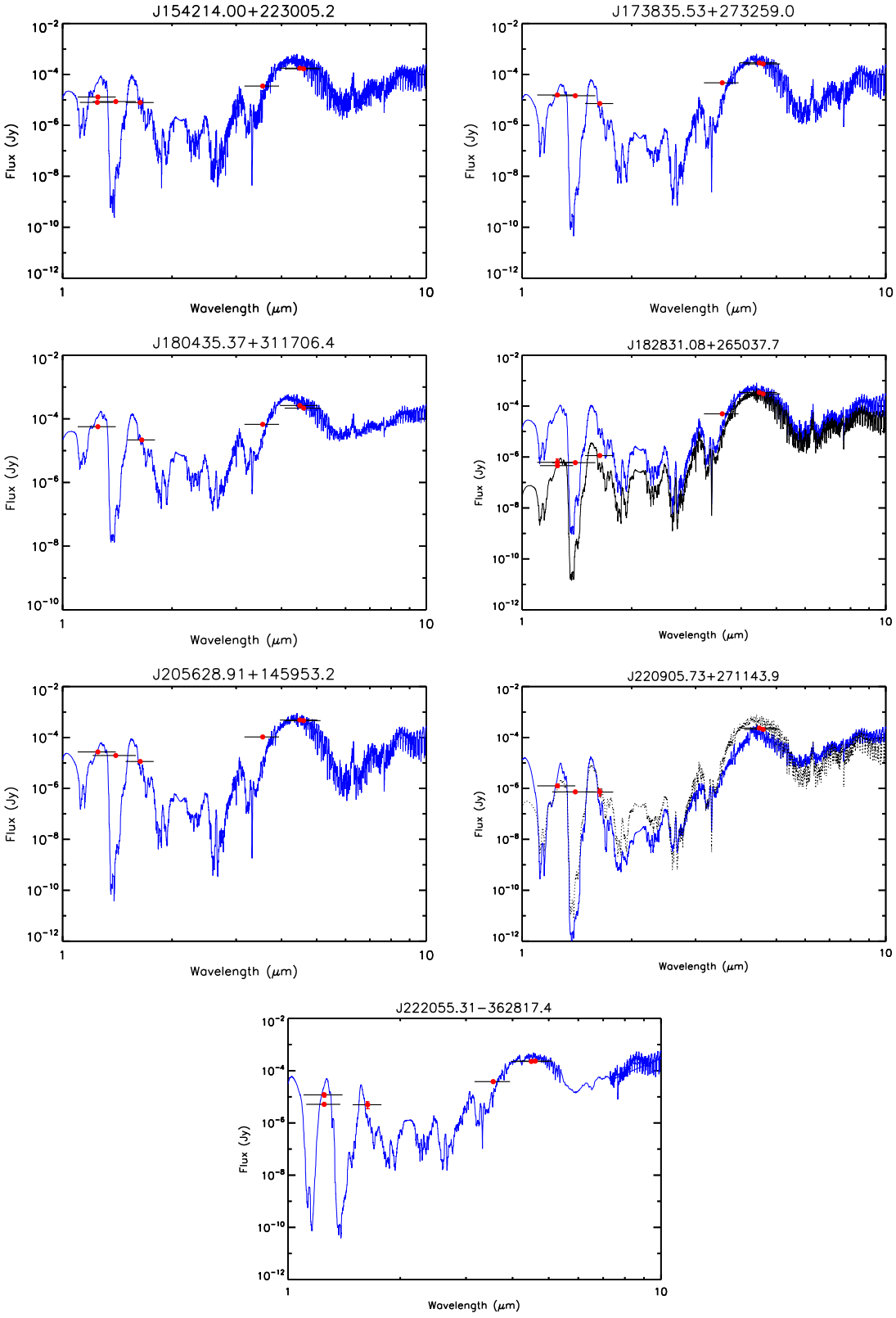


Fig. 27.— i-o). The result of fitting the photometric colors and absolute absolute 4.5 μm brightness to the BT-Settl models as described in the text. For WISE1828+2650 and WISE 2209+2711, the dotted line shows a model with added interstellar extinction as described in the text.

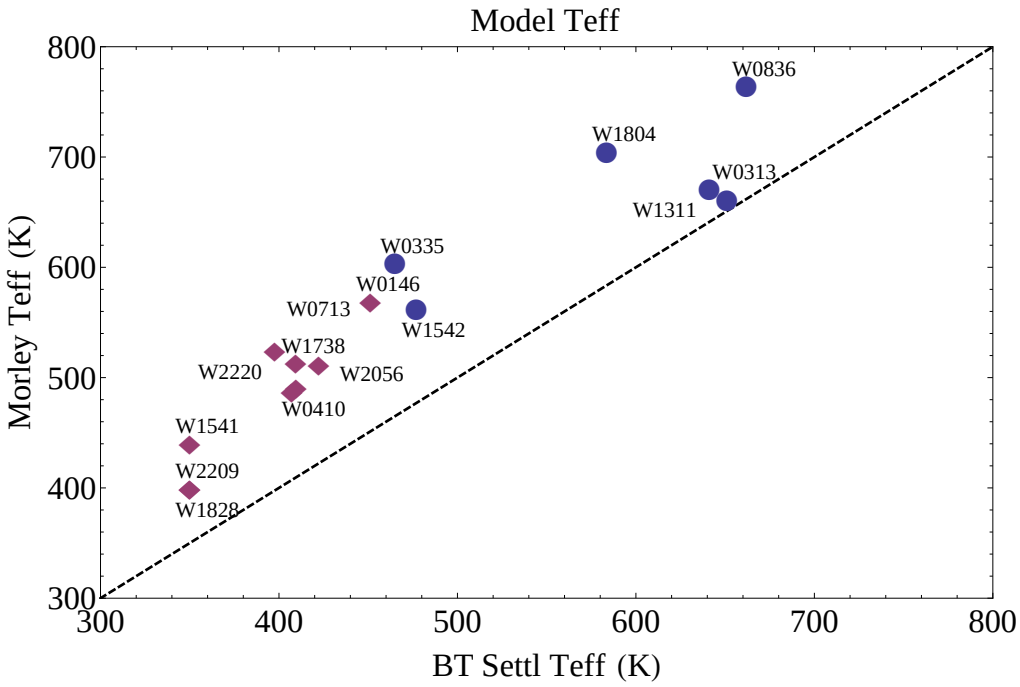


Fig. 28.— left) Comparison of best fitting effective temperatures, T_{eff} for BTSettl and Morley models. The temperatures of the Morley models are ∼75 K warmer than the corresponding BT-Settl model. The Y dwarfs are indicated by diamonds and the T dwarfs by circles and are on average ∼ 80 K cooler than the T dwarfs.

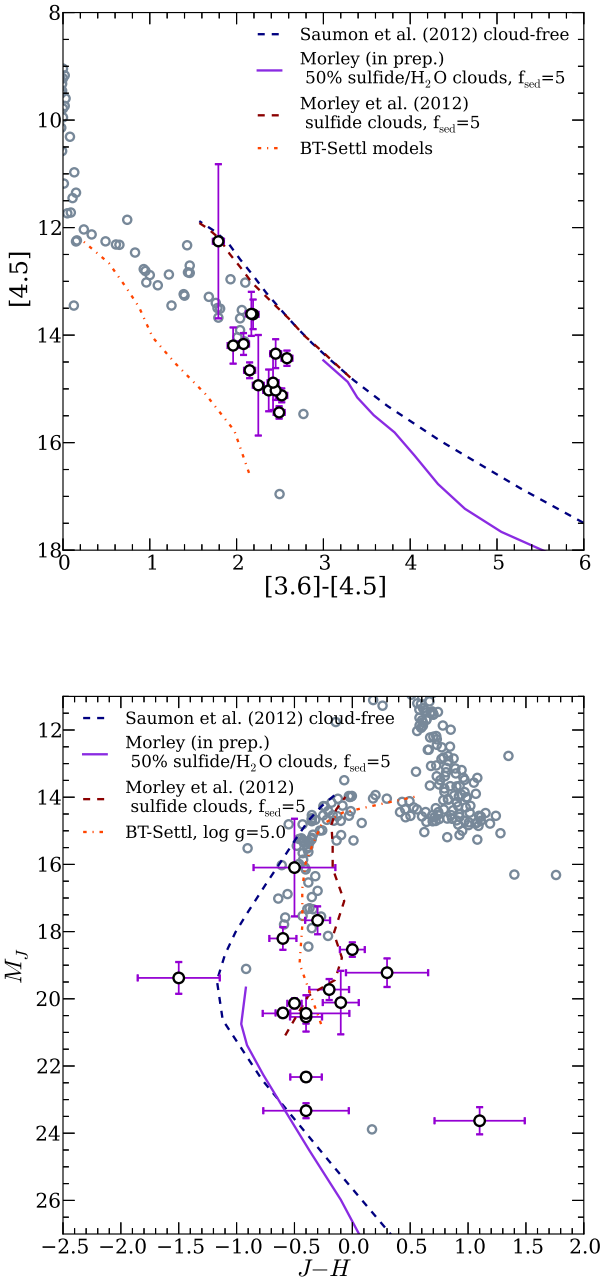


Fig. 29.— top) A Color-Magnitude diagram (CMD) for the two Spitzer bands showing a variety of models, including BT-Settl (orange, dot-dashed) and a variety of Morley models. The late T and Y dwarfs presented in this paper are plotted as well a large number of earlier spectral types taken from the literature. Three varieties of Morley models are shown, one cloud-free, one with sulfide clouds (f_{sed}=5, Table 10) and one incorporating water clouds (Morley et al in preparation). bottom) A near-IR CMD for the same set of models. The BT-Settl models provide a good fit to the J-H colors and absolute magnitudes for the warmer objects, while the Morley objects do a better job on the colder objects at these wavelengths. WISE 1828+2650 stands out as extremely red in J-H and is poorly fitted in any of the models.